neuron loss in SOD1^{H46R} ALS mice, we immunostained the lumbar sections of the spinal cord with anti-Iba-1 (marker for activated microglia) and anti-GFAP (marker for astrocytes) antibodies. At an early pre-symptomatic stage (13 weeks), there were no apparent differences in the immunoreactivity for either Iba-1 or GFAP in the lumbar spinal cord between non-transgenic, vehicle-treated SOD1^{H46R}, and L-745,870-treated SOD1^{H46R} mice (data not shown). In contrast, at 22 weeks of age (late symptomatic stage), vehicle-treated SOD1^{H46R} mice showed marked immunoreactivities both for Iba-1 and GFAP throughout the white and gray matters of the spinal cord with predominant localization in the anterior horn (Fig. 5E and H), where motor neurons were degenerated (Fig. 5B), while the lumbar spinal cord of non-transgenic siblings was almost devoid of those immunoreactivities (Fig. 5D and G). The results suggest a broad glial activation in the spinal cord of SOD1^{H46R} mice at this stage. Remarkably, L-745,870-treated SOD1^{H46R} mice showed a much less Iba-1 immunoreactivity in both white and gray matter of the anterior horn (Fig. 5F) and conservation of motor neurons (Fig. 5C) compared with vehicle-treated SOD1^{H46R} mice (Fig. 5B and E). However, there were no observable differences in immunoreactivities for GFAP, representing a diffused astrocytic proliferation in both groups (Fig. 5H and I). Immunoblot analysis also showed the decreased levels of Iba-1 in L-745,870-treated SOD1^{H46R} mice (data not shown). These results indicate that the L-745,870 treatment preferentially suppresses microglial activation, but not astrocytosis, in the spinal cord of SOD1^{H46R} mice.

The L-745,870 treatment suppresses the expression of pro-inflammatory factor

To confirm whether the L-745,870 treatment suppresses the expression of pro-inflammatory factor, we carried out immunostaining of the lumbar sections from spinal cord of SOD1^{H46R} ALS mice using anti-TNF-α antibody (Fig. 5J, K, and L). At 19 weeks of age, vehicle-treated SOD1^{H46R} mice showed marked immunoreactivities for TNF-α (Fig. 5K) particularly in large anterior horn cells, which was consistent with the recent findings (Bigini et al., 2008; Petri et al., 2007), compared with those in non-transgenic littermates (Fig. 5J). Notably, the TNF-α immunoreactivity in the corresponding region of L-745,870-treated SOD1^{H46R} mice was reduced (Fig. 5L). These results indicate that the L-745,870 treatment preferentially suppresses the expression of pro-inflammatory factor, such as TNF-α, in the spinal cord of SOD1^{H46R} mice.

We further assessed whether the L-745,870 treatment suppresses the protein oxidation in the spinal cord of SOD1^{H46R} ALS mice. Although the lumbar sections were broadly immunostained with anti-nitrotyrosine antibody, there were no significant differences of their immunoreactivities between vehicle-treated and L-745,870-treated SOD1^{H46R} mice (data not shown).

The post-onset administration of L-745,870 prolongs survival of SOD1^{H46R} mice

It is extremely crucial to evaluate whether the post-onset administration of L-745,870 improves disease symptoms. To address this issue, we conducted a daily administration of L-745,870 to SOD1^{H46R} mice after showing signs of onset (125.9±2.8 days) and observed disease progression and survival. The mean life spans (± SD) of the mice treated with 4 mg/kg, 10 mg/kg and 20 mg/kg of L-745,870 were 170.9±11.1, 173.9±7.9, and 171.4±8.5 days, respectively, and significantly extended when compared with sham (161.5±9.8 days) or vehicle-treated group (162.1±11.6 days) (Fig. 6A). Further, survival intervals in L-745,870-treated animals at doses of 4 mg/kg, 10 mg/kg, and 20 mg/kg (45.7±10.2, 47.6±7.3 and 44.1±8.5 days, respectively) significantly extended longer than those in sham (35.8±9.9 days) or vehicle-treated (35.7±10.7 days) mice (Fig. 6B), and were consistent with the results of the pre-onset administration of L-745,870 (Fig. 2C). The results also showed that 10 mg/kg of L-745,870 was an optimal dosage for exerting a potent neuroprotective efficacy in these experimental conditions. Thus, the post-onset administration of L-745,870 might effectively improve the disease symptoms and delays the disease progression in SOD1^{H46R} mice.

To further assess the effect of L-745,870 on symptoms, a rotarod test was conducted using the mice treated with L-745,870 after the onset. Although no statistically significant differences between vehicle control (n=4) and L-745,870-treated mice (n=4) were observed, there was a tendency showing that the motor function of L-745,870-treated mice was preserved when compared with that of vehicle control (Fig. 6C).

Discussion

ALS is a fatal neurodegenerative disease, and there are almost no effective therapeutic strategies to cure and/or relieve symptoms and improve the quality of life for patients to date. Although the mechanisms for the selective degeneration of motor neurons are still unclear, a complex interplay between multiple pathological factors, including oxidative stress, excitotoxicity, mitochondrial dysfunction, neurofilament accumulation, neural inflammation, and protein misfolding (Barber et al., 2006; Cluskey and Ramsden, 2001; Leichsenring et al., 2006; Menzies et al., 2002; Pasinelli and Brown, 2006; Shaw, 2005), is thought to associate with pathogenesis for ALS, and thus these factors are currently proposed as therapeutic targets. Among these pathogenic factors, there is substantial evidence to support the hypothesis that oxidative stress is one of the major processes implicating in the progression of motor neuron loss (Barber et al., 2006). This study aimed to explore the novel therapeutic agent which could alleviate oxidative stress-induced neural cell damage in ALS.

The small compound L-745,870, which is a dopamine D4 receptor antagonist having an excellent oral bioavailability and brain penetration, was firstly identified as a drug candidate for antipsychotic treatment (Patel et al., 1997). However, phase IIa clinical trials of L-745,870 failed to show clinical efficacy in patients with acute schizophrenia (Bristow et al., 1997). On the other hand, we previously reported that L-745,870 selectively inhibited cell death induced by oxidative stress *in vitro* and exerted a potent neuroprotective effect *in vivo* acute ischemic model (Okada et al., 2005). In the present study, we sought to examine whether the chronic administration of L-745,870 effectively attenuates motor neuron loss in a SOD1^{H46R} ALS mouse model. We here demonstrated that the pre-onset administration of L-745,870 significantly retarded the disease-onset and prolonged survival in transgenic SOD1^{H46R} mice. The L-745,870 treatment also delayed loss of motor neurons in the spinal cord accompanying with the reduced level of microglial activation. Most importantly, the post-onset administration of L-745,870 resulted in a slowed progression in a same mouse ALS model.

Currently, the pharmaco-mechanisms by which L-745,870 protects motor neuron loss are still unclear. In order to investigate the mode of action of L-745,870 *in vitro*, we previously performed cell viability analyses against cell death induced by various stimuli including oxidative stressors by utilizing non-neuronal (HeLa, THP-1, and fibroblast) and neuronal (SH-SY5Y) cell cultures. As a result, the L-745,870-treatment comparatively protected all examined cell types from death induced by oxidative stressors such as menadione and H_2O_2, but not by other stimuli such as staurosporine and okadaic acid (Okada et al., 2005), suggesting that L-745,870 selectively inhibited oxidative stress-induced cell death in a cell type-independent fashion. It has been reported that the several types of dopamine receptors are expressed in SH-SY5Y cells, but not in HeLa cells (Kamakura et al., 1997; Presgraves et al., 2004). Thus, L-745,870 seems to be effective to the cells irrespective to the expression of dopamine receptors. In other words, the mode of action of this compound could be dopamine receptor-independent, although we could not completely rule out the possibility that L-745,870 exerts its potency via dopamine receptors. Alternatively, as we have originally identified L-745,870 as a NAIP-upregulating compound (Okada et al., 2005), and NAIP is known to

exert potent neuroprotective activity against oxidative stress-induced cell death (Liston et al., 1996), it is reasonable that L-745,870 exerts its potency by enhancing the NAIP-mediated cellular protection from oxidative stress in transgenic SOD1^{H46R} mice.

Several lines of evidence have demonstrated that both microglia and astrocyte were proliferated in the affected regions of ALS patients and mutant SOD1 mouse ALS models (Hall et al., 1998; Kawamata et al., 1992; Schiffer et al., 1996). Two independent groups have reported that astrocytes have an impact on motor neuron degeneration (Di Giorgio et al., 2007; Nagai et al., 2007), while others have reported that microglia contribute to non-cell-autonomous damage of neurons in neurodegenerative diseases (Block et al., 2007; Liu and Hong, 2003; Moisse and Strong, 2006). Further, it has also been proposed that chromogranin-mediated secretion of mutant SOD1 from neurons and astrocytes enhances microgliosis and motor neuron death (Urushitani et al., 2006). These studies suggest a contribution of non-neuronal cells to the ALS pathogenesis. In the present study, we showed that L-745,870 suppressed the activation of microglia, but not astrocytosis, in the spinal cord of SOD1^{H46R} mice. Further, L-745,870 suppresses the upregulation of pro-inflammatory factor (TNF-α) but not the oxidative modification of proteins (nitrated proteins) in motor neurons. Recently, it has been reported that the activation of NADPH oxidase generating ROS from microglia promotes motor neuron degeneration in the spinal cord (Wu et al., 2006). NADPH oxidase, which is a membrane-bound enzyme and catalyzes the production of superoxide from oxygen, has been implicated as an important source of microglial-derived ROS generation (Block et al., 2007). It has also been shown that the production of pro-inflammatory factors is induced by ROS (Barber et al., 2006). Thus, the L-745,870 treatment may attenuate the microglia activation and coordinately suppress the expression of TNF-α in the spinal cord, which in turn results in the protection from motor neuron loss.

In conclusions, our findings in a rodent model of ALS, demonstrating an obvious neuroprotective efficacy of L-745,870, may have implication that L-745,870 is a promising candidate as a potential therapeutic drug to the treatment of ALS. Moreover, as reactive microglia have identified in the spinal cord from sporadic ALS patients (Kawamata et al., 1992), L-745,870 might be useful not only for familial but also for sporadic ALS. Although the mode of action of L-745,870 on motor neuron protection is not fully understood, future studies on the target analysis of L-745,870 *in vivo* will clarify more therapeutic potential of L-745,870 in ALS and other neurodegenerative diseases.

Acknowledgments

This work was funded by the Ministry of Health, Labour and Welfare (J.E.I.), and partly by the National Institute of Biomedical Innovation (NIBIO) (J.E.I.).

References

Alexianu, M.E., Kozovska, M., Appel, S.H., 2001. Immune reactivity in a mouse model of familial ALS correlates with disease progression. Neurology 57, 1282–1289.

Barber, S.C., Mead, R.J., Shaw, P.J., 2006. Oxidative stress in ALS: a mechanism of neurodegeneration and a therapeutic target. Biochim. Biophys. Acta 1726, 1051–1067.

Bigini, P., Repici, M., Cantarella, G., Fumagalli, E., Barbera, S., Cagnotto, A., De Luigi, A., Tonelli, R., Bernardini, R., Borsello, T., Mennini, T., 2008. Recombinant human TNF-binding protein-1 (rhTBP-1) treatment delays both symptoms progression and motor neuron loss in the wobbler mouse. Neurobiol. Dis. doi:10.1016/j.nbd.2007.11.005.

Block, M.L., Zecca, L., Hong, J.-S., 2007. Microglia-mediated neurotoxicity: uncovering the molecular mechanisms. Nat. Rev. Neurosci. 8, 57–69.

Bristow, L.J., Kramer, M.S., Kulagowski, J., Patel, S., Ragan, C.I., Seabrook, G.R., 1997. Schizophrenia and L-745,870, a novel dopamine D4 receptor antagonist. Trends Pharmacol. Sci. 18, 186–188.

Chang-Hong, R., Wada, M., Koyama, S., Kimura, H., Arawaka, S., Kawanami, T., Kurita, K., Kadoya, T., Aoki, M., Itoyama, Y., Kato, T., 2005. Neuroprotective effect of oxidized galectin-1 in a transgenic mouse model of amyotrophic lateral sclerosis. Exp. Neurol. 194, 203–211.

Cleveland, D.W., Rothstein, J.D., 2001. From Charcot to Lou Gehrig: deciphering selective motor neuron death in ALS. Nat. Rev. Neurosci. 2, 806–819.

Cluskey, S., Ramsden, D.B., 2001. Mechanisms of neurodegeneration in amyotrophic lateral sclerosis. J. Clin. Pathol: Mol. Pathol. 54, 386–392.

Di Giorgio, F.P., Carrasco, M.A., Siao, M.C., Maniatis, T., Eggan, K., 2007. Non-cell autonomous effect of glia on motor neurons in an embryonic stem cell-based ALS model. Nat. Neurosci. 10, 608–614.

Hall, E.D., Oostveen, J.A., Gurney, M.E., 1998. Relationship of microglial and astrocytic activation to disease onset and progression in a transgenic model of familial ALS. Glia 23, 249–256.

Heiman-Patterson, T.D., Deitch, J.S., Blankenhorn, E.P., Erwin, K.L., Perreault, M.J., Alexander, B.K., Byers, N., Toman, I., Alexander, G.M., 2005. Background and gender effects on survival in the TgN(SOD1-G93A)1Gur mouse model of ALS. J. Neurol. Sci. 236, 1–7.

Kamakura, S., Iwaki, A., Matsumoto, M., Fukumaki, Y., 1997. Cloning and characterization of the 5′-flanking region of human dopamine D4 receptor gene. Biochem. Biophys. Res. Commun. 235, 321–326.

Kawamata, T., Akiyama, H., Yamada, T., McGeer, P.L., 1992. Immunologic reactions in amyotrophic lateral sclerosis brain and spinal cord tissue. Am. J. Pathol. 140, 691–707.

Kim, N.H., Jeong, M.S., Choi, S.Y., Kang, J.H., 2004. Oxidative modification of neurofilament-L by the Cu,Zn-superoxide dismutase and hydrogen peroxide system. Biochimie 86, 553–559.

Kriz, J., Nguyen, M.D., Julien, J.-P., 2002. Minocycline slows disease progression in a mouse model of amyotrophic lateral sclerosis. Neurobiol. Dis. 10, 268–278.

Leichsenring, A., Linnartz, B., Zhu, X.R., Lübbert, H., Stichel, C.C., 2006. Ascending neuropathology in the CNS of a mutant SOD1 mouse model of amyotrophic lateral sclerosis. Brain Res. 1096, 180–195.

Liston, P., Roy, N., Tamai, K., Lefebvre, C., Baird, S., Cherton-Horvat, G., Farahani, R., McLean, M., Ikeda, J.-E., MacKenzie, A., Korneluk, R.G., 1996. Suppression of apoptosis in mammalian cells by NAIP and a related family of IAP genes. Nature 379, 349–353.

Liu, B., Hong, J.-S., 2003. Role of microglia in inflammation-mediated neurodegenerative diseases: mechanisms and strategies for therapeutic intervention. J. Pharmacol. Exp. Ther. 304, 1–7.

Menzies, F.M., Ince, P.G., Shaw, P.J., 2002. Mitochondrial involvement in amyotrophic lateral sclerosis. Neurochem.Int. 40, 543–551.

Moisse, K., Strong, M.J., 2006. Innate immunity in amyotrophic lateral sclerosis. Biochim. Biophys. Acta 1726, 1083–1093.

Nagai, M., Re, D.B., Nagata, T., Chalazonitis, A., Jessell, T.M., Wichterle, H., Przedborski, S., 2007. Astrocytes expressing ALS-linked mutated SOD1 release factors selectively toxic to motor neurons. Nat. Neurosci. 10, 615–622.

Okada, Y., Sakai, H., Kohiki, E., Suga, E., Yanagisawa, Y., Tanaka, K., Hadano, S., Osuga, H., Ikeda, J.-E., 2005. A dopamine D4 receptor antagonist attenuates ischemia-induced neuronal cell damage via upregulation of neuronal apoptosis inhibitory protein. J. Cereb. Blood Flow Metab. 25, 794–806.

Pasinelli, P., Brown, R.H., 2006. Molecular biology of amyotrophic lateral sclerosis: insights from genetics. Nat. Rev. Neurosci. 7, 710–723.

Patel, S., Freedman, S., Chapman, K.L., Emms, F., Fletcher, A.E., Knowles, M., Marwood, R., Mcallister, G., Myers, J., Curtis, N., Kulagowski, J.J., Leeson, P.D., Ridgill, M., Graham, M., Matheson, S., Rathbone, D., Watt, A.P., Bristow, L.J., Rupniak, N.M., Baskin, E., Lynch, J.J., Ragan, C.I., 1997. Biological profile of L-745,870, a selective antagonist with high affinity for the dopamine D4 receptor. J. Pharmacol.Exp. Ther. 283, 636–647.

Petri, S., Calingasan, N.Y., Alsaied, O.A., Wille, E., Kiaei, M., Friedman, J.E., Baranova, O., Chavez, J.C., Beal, M.F., 2007. The lipophilic metal chelators DP-109 and DP-460 are neuroprotective in a transgenic mouse model of amyotrophic lateral sclerosis. J. Neurochem. 102, 991–1000.

Presgraves, S.P., Borwege, S., Millan, M.J., Joyce, J.N., 2004. Involvement of dopamine D(2)/D(3) receptors and BDNF in the neuroprotective effects of S32504 and pramipexole against 1-methyl-4-phenylpyridinium in terminally differentiated SH-SY5Y cells. Exp. Neurol. 190, 157–170.

Rao, S.D., Yin, H.Z., Weiss, J.H., 2003. Disruption of glial glutamate transport by reactive oxygen species produced in motor neurons. J. Neurosci. 23, 2627–2633.

Rao, S.D., Weiss, J.H., 2004. Excitotoxic and oxidative cross-talk between motor neurons and glia in ALS pathogenesis. Trends Neurosci. 27, 17–23.

Rosen, D.R., Siddique, T., Patterson, D., Figlewicz, D.A., Sapp, P., Hentati, A., Donaldson, D., Goto, J., O'Regan, J.P., Deng, H.-X., Rahmani, Z., Krizus, A., McKenna-Yasek, D., Cayabyab, A., Gaston, S.M., Berger, R., Tanzi, R.E., Halperin, J.J., Herzfeldt, B., Van den Bergh, R., Hung, W.-Y., Bird, T., Deng, G., Mulder, D.W., Smyth, C., Laing, N.G., Soriano, E., Pericak-Vance, M.A., Haines, J., Rouleau, G.A., Gusella, J.S., Horvitz, H, Brown Jr., R. R.H., 1993. Mutations in Cu/Zn superoxide dismutase gene are associated with familial amyotrophic lateral sclerosis. Nature 362, 59–62.

Sasaki, S., Nagai, M., Aoki, M., Komori, T., Itoyama, Y., Iwata, M., 2007. Motor neuron disease in transgenic mice with an H46R mutant *SOD1* gene. J. Neuropathol. Exp. Neurol. 66, 517–524.

Schiffer, D., Cordera, S., Cavalla, P., Migheli, A., 1996. Reactive astrogliosis of the spinal cord in amyotrophic lateral sclerosis. J. Neurol. Sci. 139 (Suppl.), 27–33.

Shaw, P.J., 2005. Molecular and cellular pathways of neurodegeneration in motor neurone disease. J. Neurol. Neurosurg. Psychiatry 76, 1046–1057.

Trotti, D., Rolfs, A., Danbolt, N.C., Brown Jr., R.H., Hediger, M.A., 1999. SOD1 mutants linked to amyotrophic lateral sclerosis selectively inactivate a glial glutamate transporter. Nat. Neurosci. 2, 427–433.

Urushitani, M., Sik, A., Sakurai, T., Nukina, N., Takahashi, R., Julien, J.-P., 2006. Chromogranin-mediated secretion of mutant superoxide dismutase proteins linked to amyotrophic lateral sclerosis. Nat. Neurosci. 9, 108–118.

Wu, D.-C., Ré, D.B., Nagai, M., Ischiropoulos, H., Przedborski, S., 2006. The inflammatory NADPH oxidase enzyme modulates motor neuron degeneration in amyotrophic lateral sclerosis mice. Proc. Natl. Acad. Sci. U.S.A. 103, 12132–12137.

J Neuropathol Exp Neurol

Vol. 68, No. 4
April 2009
pp. 365–373

ORIGINAL ARTICLE

Mitochondrial Alterations in Transgenic Mice With an H46R Mutant Cu/Zn Superoxide Dismutase Gene

Shoichi Sasaki, MD, Masashi Aoki, MD, Makiko Nagai, MD,
Makio Kobayashi, MD, and Yasuto Itoyama, MD

Abstract

We examined morphological alterations in the mitochondria in the spinal cord of H46R mutant Cu/Zn superoxide dismutase transgenic mice; these mice serve as a model for human familial amyotrophic lateral sclerosis. The disease in the mice is characterized by initial muscle weakness and atrophy in the legs, very long clinical courses, and widespread pathological changes of the spinal cord that extends beyond the motor system and includes many neuropil aggregates that lack vacuoles. At the preclinical stage, we found alterations in the mitochondrial cristae that included focal electron-dense changes, whorled membranous and electron-dense amorphous structures, and outward projections of outer and inner membranes predominantly in proximal axons. At the overt disease stage, these mitochondrial alterations were more frequent and were also found in somata, dendrites, presynaptic terminals, and astrocyte cytoplasm. By immunoelectron microscopy, no accumulations of Cu/Zn superoxide dismutase– or ubiquitin-positive immunogold particles were observed in either normal-appearing or abnormal mitochondria. These findings suggest that predominant mitochondrial alterations in the proximal axons begin in the preclinical stage and may be involved in the pathogenetic mechanisms of motor neuron degeneration in these transgenic mice via disruption of the axonal transport of substrates necessary for neuronal viability; this disruption may lead to motor neuron death.

Key Words: Aggregates, Amyotrophic lateral sclerosis, Astrocytes, H46R, Mitochondria, SOD1, Transgenic mice.

INTRODUCTION

Familial amyotrophic lateral sclerosis (FALS) with a novel point mutation (H46R) in exon 2 of the Cu/Zn superoxide dismutase (*SOD1*) gene is an autosomal dominant disorder that has been reported in the Japanese population. Patients with FALS who have an H46R SOD1 mutation are characterized clinically as having a "pseudopolyneuritic form of amyotrophic lateral sclerosis (ALS)," that is, with lower motor neuron-dominant involvement developing in the lower extremities and remarkably long clinical courses of approximately 15 years (1–3). Transgenic (Tg) mice with this mutation exhibit widespread changes that extend beyond the motor system to involve the entire white matter of the spinal cord and the anterior and posterior roots; these findings are accompanied by numerous SOD1- and ubiquitin-positive aggregates lacking vacuoles in the neuropil (4). Recently, accumulating evidence has indicated that mitochondrial damage is involved in motor neuron degeneration in sporadic ALS (5–7), FALS with a SOD1 mutation (8, 9), and in mutant SOD1 Tg mice (10, 11). There, currently, is no information, however, on morphological alterations in the mitochondria of H46R mutant SOD1 Tg mice. This is the first report to focus on the fine structural alterations of mitochondria in motor neurons and their neuronal processes and astrocytes in H46R mutant SOD1 Tg mice.

MATERIALS AND METHODS

Experimental Animals and Clinical Assessment

All mice were handled according to approved animal protocols of the Tohoku University Graduate School of Medicine (the Recombinant DNA Experiment Safety Committee including Animal Experimental Committee). The processes of development and clinical assessment of H46R mutant SOD1 Tg mice have been previously reported (4). Briefly, the DNA of newborn mice was extracted from their tails, and polymerase chain reaction amplification (forward primer: 5′-TTGGG AGGAGGTAGTGATTA; reverse primer: 5′-AGCTAGCAG GATAACAGATGA; 94°C for 30 seconds; 55°C for 30 seconds; 72°C for 30 seconds; 30 cycles) and Southern blotting were used to detect the exogenous human *SOD1* transgene.

To generate Tg mice with the H46R mutation, we first obtained human genomic PAC clones encompassing the entire human *SOD1* gene; we then subcloned this gene within an 11.5-kb *Eco*RI-*Bam*HI fragment. Site-directed mutagenesis was used to generate clones with the H46R mutation. The mutated 11.5-kb *Eco*RI-*Bam*HI fragments were microinjected into fertilized eggs from BDF1 mice; 83 potential Tg H46R pups were obtained. From these, 3 founders with the H46R mutant transgene were identified using polymerase chain reaction

From the Department of Neurology (SS), Tokyo Women's Medical University, Tokyo; Department of Neurology (MA, YT), Tohoku University Graduate School of Medicine, Sendai; Department of Neurology (MN), Okayama University, Okayama; and Department of Pathology (MK), Tokyo Women's Medical University, Tokyo, Japan.

Send correspondence and reprint requests to: Shoichi Sasaki, MD, Department of Neurology, Tokyo Women's Medical University, 8-1 Kawada-cho, Shinjuku-ku, Tokyo 162-8666, Japan; E-mail: ssasaki@nij.twmu.ac.jp

This work was supported by a Grant-in-Aid for General Scientific Research (C) (18500280) from The Ministry of Education, Culture, Sports, Science and Technology; a grant from the Japan Amyotrophic Lateral Sclerosis Association; and grants from the Ministry of Health, Labor and Welfare in Japan.

and Southern blotting. One line with the H46R mutation developed motor neuron disease. This line expressed the highest level of the mutant SOD1.

The first sign of disease in this mutant line was weakness of limbs that was primarily indicated by the dragging of 1 limb. In the H46R-70 line, all of the mice showed weakness in their hind limbs. The mean age at which this clinical weakness appeared was 153 ± 10.0 days (n = 4). As the disease progressed, the mice exhibited marked muscle wasting in their limbs. Thereafter, the other limbs also became weak. At the end stage of disease, the affected mice were unable to move toward water to drink and they died. The mean ages at death in the H46R-70 line was 184 ± 11.8 days (n = 4). The mean duration of the clinical expression of the disease in the H46R-70 was 27.5 ± 8.2 days (n = 4). The lines that expressed lower levels of human mutant SOD1 did not show any clinical signs up to 12 months of age. A total of 19 Tg mice and 18 nontransgenic (non-Tg) mice were studied.

Histopathology

Eight Tg mice and 8 age-matched non-Tg mice were studied by histopathology. The Tg mice were divided into 4 groups as follows: early preclinical (aged 12 weeks, n = 2), late preclinical (16 weeks, n = 2), early clinical (20 weeks, n = 2), and end-stage (24 weeks, n = 2) Tg mice. Age-matched non-Tg mice served as controls in each group; Tg and non-Tg mice were examined at the same time. The mice were deeply anesthetized with ether and perfused intracardially with heparinized saline (pH 7.4), followed by perfusion with ice-cold 4% paraformaldehyde (Katayama Chemical, Osaka, Japan) in 0.1 M phosphate buffer (pH 7.4). The spinal cords were removed rapidly and postfixed by immersion in the same fixative (5 days, 4°C). Cross-sections of the spinal cord were embedded in paraffin, sectioned (4 μm), and subsequently stained with hematoxylin and eosin (H&E) and with Klüver-Barrera stain.

Electron Microscopy

Eight Tg and 8 non-Tg wild-type mice were killed at ages 12, 16, 20, and 24 weeks (n = 2 in each group, respectively). All mice were perfused intracardially with heparinized saline (pH 7.4), followed by perfusion with ice-cold 4% paraformaldehyde (Katayama Chemical) and 0.2% glutaraldehyde in 0.1 M phosphate buffer (pH 7.4). Tissues of the spinal cord were incubated in 2% osmium tetroxide in 0.1 M cacodylate for 2 hours, washed, dehydrated, and embedded in epoxy resin. Serial semithin sections (1 μm thick) of the whole transverse spinal cord stained with toluidine blue were examined under a light microscope. The spinal cord sections (including the anterior and posterior horns, anterior, lateral and posterior columns, and anterior and posterior roots) were cut into ultrathin sections that were subsequently stained with uranyl acetate and lead citrate.

Semiquantitative analysis of the incidence of abnormal mitochondria was performed in 1,000 normal-appearing myelinated axons with a diameter of more than 3 μm (i.e. the mean of the shortest and the largest diameters of an axon) within the anterior column of the lumbar spinal cord at each stage of Tg mice, respectively, making a total of 4,000 myelinated axons.

Immunoelectron Microscopy

Postembedding immunogold electron microscopy was carried out on spinal cord specimens. Late preclinical (16 weeks, n = 1), early clinical (20 weeks, n = 1), and end-stage (24 weeks, n = 1) mice were perfused as described above for electron microscopy. Two non-Tg wild-type mice (20 weeks, n = 1; 24 weeks, n = 1) served as controls. The lumbar and cervical spinal cords were dissected out, dehydrated in 100% ethanol, and embedded in hard-grade LR White resin (Electron Microscopy Sciences, Fort Washington, PA) by polymerization overnight at 60°C. Ultrathin sections were excised from the embedded tissue using a microtome and were collected onto grids (150 mesh). The ultrathin sections were then etched in 0.1 N HCl for 5 minutes, rinsed 3 times for 5 minutes each in Tris-buffered saline (TBS) (20 mM Tris, 140 mM NaCl, and 2.7 mM KCl, pH 8.0), treated with blocking buffer (0.1% gelatin, 1% normal goat serum, and 0.3% Triton-X-100 in TBS) for 30 minutes, incubated with the primary antibodies for 2 hours at room temperature, rinsed 3 times for 5 minutes each in TBS, placed in gold-conjugated secondary antibody (10-nm gold anti-mouse anti-rabbit) for 1 hour, rinsed 3 times in TBS, rinsed in water, and stained with uranyl acetate and lead citrate. The following antibodies and sera were used: sheep polyclonal anti-human SOD1 antibody (Calbiochem, San Diego, CA) at 1:500, 1:1000, or 1:2000 dilution; a polyclonal anti-ubiquitin antibody (DAKO, Carpinteria, CA) diluted at 1:100, 1:500, or 1:1000; and a monoclonal anti-phosphorylated neurofilament antibody (DAKO) diluted at 1:50, 1:100, 1:500, and normal rabbit serum (Vector Laboratories, Burlingame, CA).

RESULTS

Light Microscopic Findings

Light microscopic findings have been previously reported (4). Briefly, in 12-week-old (early preclinical stage) mice, H&E and Klüver-Barrera staining revealed no pathological changes anywhere in the spinal cord. In Epon-embedded plastic sections stained with toluidine blue, however, there were rare aggregates detected in the neuropil of the anterior horns and around the central canal but not in the posterior horns or white matter. The anterior and posterior roots showed no abnormalities.

In 16-week-old (late preclinical stage) mice, H&E and Klüver-Barrera staining revealed no pathological changes in either the gray matter or the white matter, and no neuronal loss was observed anywhere in the spinal cord; SOD1- and ubiquitin-positive inclusions without cores (aggregates) and eosinophilic, SOD1- and ubiquitin-positive inclusions with cores (Lewy body-like inclusions [LIs]) were, however, rarely observed by H&E staining. In plastic sections, aggregates, LIs, spheroids, and cord-like swollen axons were occasionally seen in the neuropil in the anterior horns. Myelin ovoids were only occasionally observed in all white matter examined, but the anterior and posterior roots were intact.

In 20-week-old (early clinical stage) and 24-week-old (end stage) mice, the average numbers of large anterior horn neurons were significantly less than in the controls. Aggregates and LIs were frequently observed in the neuropil of the anterior horn. In plastic sections, aggregates, LIs, spheroids,

and cord-like swollen axons were frequently seen in the neuropil of the anterior horns. Aggregates and LIs were also observed in the posterior horns and in the white matter of the anterior, lateral, and posterior columns at the end stage. Swollen axons (spheroids) were prominent at the exit zone of the anterior roots in the anterior columns as well as in the anterior horns. Myelin ovoids and degenerated fibers were prominent in the anterior roots and posterior roots, as well as in the white matter of the anterior, lateral, and posterior columns, including in the pyramidal tract over time. No vacuolar changes were observed anywhere at any stage of disease progression.

Electron Microscopic Findings

Non-Tg littermates

Mitochondria in neuronal perikarya, dendrites, and axons were well preserved and surrounded by an outer unit membrane and an inner, folded membrane that formed the cristae; the latter were filled with a dense matrix (Fig. 1). The intermembrane space was generally lucent. Disorganization or small vacuolar changes in the inner compartment and whorled membranous structures were only occasionally seen in the spinal cord gray and white matter and the anterior and posterior roots. Electron-dense changes of cristae and electron-dense amorphous structures were rare anywhere in the spinal cord of non-Tg mice.

Tg mice

Mitochondria were also well preserved. In 12-week-old mice, mitochondria were almost always normal in structure; large, swollen mitochondria with an increased number of cristae (Fig. 2) and mitochondria with disorganized inner compartment (Fig. 3) or whorled membranous structures were only occasionally observed. These abnormalities were predominantly in the gray and white matter axons and the anterior and posterior roots and, to a lesser degree, in dendrites and somata of anterior horn neurons. Electron-dense changes of cristae were rarely found anywhere.

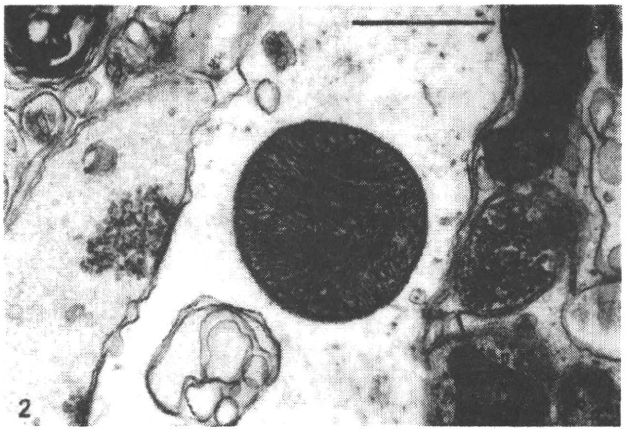

FIGURE 2. Transgenic mouse (12 weeks, early preclinical stage). A large swollen mitochondrion with an abnormally high number of cristae is seen in the dendrite of an anterior horn neuron. Scale bar = 1 μm.

In 16-week-old mice, swollen mitochondria were more numerous than in younger mice. Mitochondria with a disorganized inner compartment or whorled membranous structures were only occasionally observed in the axons of the gray and white matter and the anterior and posterior roots. Mitochondrial alterations in the cristae were occasionally observed in the proximal axons of the anterior horns.

In 20-week-old mice, enlarged mitochondria with increased numbers of cristae and mitochondria with a disorganized inner compartment were less prominent in the neuronal processes and somata of the anterior horn neurons. The intermembrane space was occasionally dilated and contained membranous structures (Fig. 4). Mitochondria with whorled membranous structures were occasionally observed in anterior and posterior horns, anterior and lateral columns,

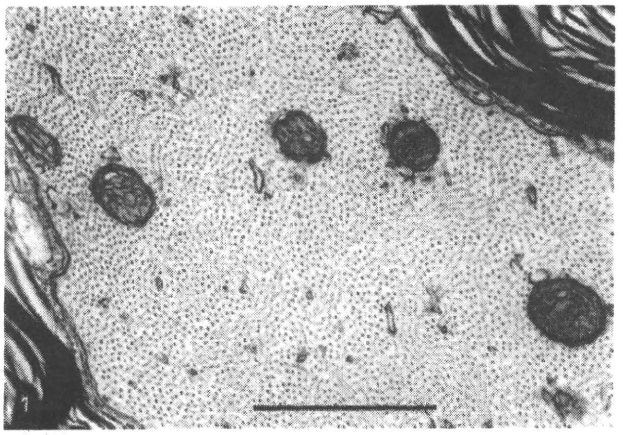

FIGURE 1. Nontransgenic littermate (24 weeks). The mitochondria in an axon are well preserved and surrounded by an outer smooth unit membrane and an inner folded membrane that forms the cristae that are filled with a dense matrix. The intermembrane space is generally lucent. Scale bar = 1 μm.

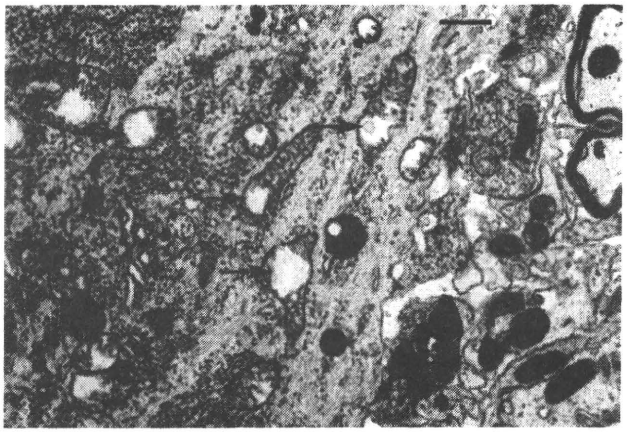

FIGURE 3. Transgenic mouse (12 weeks). The inner compartments of some mitochondria in the soma of an anterior horn neuron are disorganized and empty (arrows). Mitochondria in the presynaptic terminals and neuropil are well preserved. Scale bar = 1 μm.

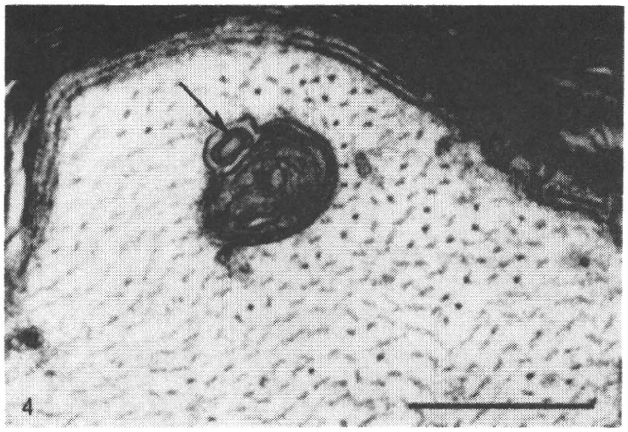

FIGURE 4. Transgenic mouse (20 weeks, early clinical stage). The intermembrane space is dilated and contains a membranous structure (arrow). Scale bar = 0.5 μm.

and anterior roots to a greater extent than in the posterior columns and roots. Alterations in the cristae, that is, focal electron-dense changes (Fig. 5) and electron-dense amorphous structures, were more frequently observed in the proximal axons of the anterior horns, the anterior and lateral columns, and the anterior roots and, to a lesser degree, the posterior horns and the posterior column than in the 16-week-old mice. Electron-dense changes of cristae were not found in the posterior roots. Slight focal, outward projections of both the inner and outer membranes were observed on both transverse and longitudinal sections (Fig. 6).

In 24-week-old mice, focal electron-dense changes in the cristae, whorled membranous structures (Fig. 7), and electron-dense amorphous structures (Fig. 8) became prominent in the anterior horns, the anterior and lateral columns, and the anterior roots and, to a lesser degree, the posterior structures; the entire interior of the mitochondria frequently appeared to be electron-dense membranous or amorphous structures (Fig. 9). These inner and outer membrane structures projected prominently outward (Fig. 10). These changes

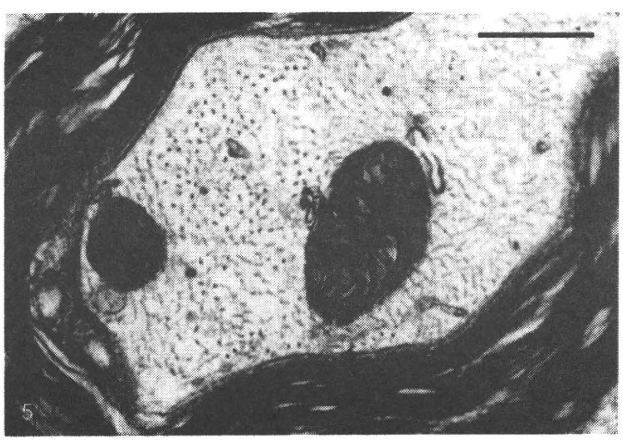

FIGURE 5. Transgenic mouse (20 weeks). There are focal electron-dense changes in the cristae of a mitochondrion in an axon. Scale bar = 0.5 μm.

FIGURE 6. Transgenic mouse (20 weeks). Inner and outer membranes are focally projected slightly outward in a longitudinal section; there are also electron-dense changes in the cristae. Scale bar = 1 μm.

were frequently observed not only in proximal axons but also in the somata of large and small anterior horn neurons, dendrites (Fig. 11), and presynaptic terminals on the surface of anterior horn cells (Fig. 12). The alterations in the cristae were more frequent in degenerative motor neurons that showed central chromatolysis than in normal-looking motor neurons at any stage. Astrocytes occasionally contained mitochondria that showed swellings, disorganization of inner compartments, and electron-dense membranous or amorphous structures of cristae in the cytoplasm at this stage (Fig. 13).

Semiquantitative Analysis of the Incidence of Abnormal Mitochondria

Mitochondrial alterations were most frequently observed in the anterior columns. Therefore, we carried out a semiquantitative analysis of the incidence of abnormal mitochondria in the anterior column of the lumbar spinal cord (Table). We investigated 1,000 normal-looking myelinated axons at each stage, making a total of 4,000 myelinated axons.

FIGURE 7. Transgenic mouse (24 weeks, end stage). There are whorled membranous structures in the outer portions of a mitochondrion in an axon. Scale bar = 0.5 μm.

FIGURE 8. Transgenic mouse (24 weeks). There are electron-dense amorphous changes in the cristae of an axonal mitochondrion. Scale bar = 0.5 μm.

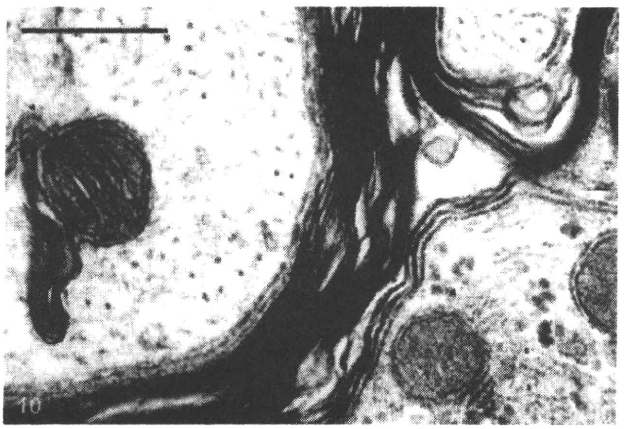

FIGURE 10. Transgenic mouse (24 weeks). Electron-dense membranous structures of the inner and outer mitochondrial membranes project prominently outward. Scale bar = 0.5 μm.

In 12-week-old mice, a total of 2,612 mitochondria were observed in 1,000 myelinated axons. The average number of mitochondria was 2.61 ± 1.80. Focal electron-dense changes in the cristae (Fig. 5) and whorled membranous structures (Fig. 7) were observed in 5 (0.19 %) and 19 (0.73 %), respectively.

In 16-week-old mice, a total of 2,611 mitochondria were observed. The average number of mitochondria was 2.61 ± 1.88. Focal electron-dense changes in the cristae and whorled membranous structures were observed in 4 (0.15 %) and 41 (1.57 %) mitochondria, respectively. The outward projection of the inner and outer membranes (Fig. 10) was observed in 5 (0.19 %).

In 20-week-old mice, a total of 1,880 mitochondria were observed. The average number of mitochondria was 1.88 ± 1.59. Alterations in the cristae such as focal electron-dense changes and electron-dense amorphous structures (Fig. 8) were observed in 60 mitochondria (3.19 %). Whorled membranous structures and the outward projection of the inner and outer membranes (Fig. 10) were observed in 44 (2.34 %) and 17 (0.90 %) mitochondria, respectively.

In 24-week-old mice, a total of 1,666 mitochondria were observed. The average number of mitochondria was 1.67 ± 1.38. Alterations in the cristae such as focal electron-dense changes and electron-dense amorphous structures were observed in 158 mitochondria (9.48 %). Whorled membranous structures and the outward projection of the inner and outer membranes were observed in 61 (3.66 %) and 5 (0.30 %) mitochondria, respectively.

Thus, the incidence of abnormal mitochondria increased from the preclinical to overt clinical stages. The incidence of whorled membranous structures and outward projection of the inner and outer membranes was significantly increased in the late preclinical stage compared with the early preclinical stage (Fisher exact test, $p < 0.05$). In the overt clinical disease stages, abnormalities of all the mitochondrial components were significantly increased compared with those in the early stage (Fisher exact test, $p < 0.01$).

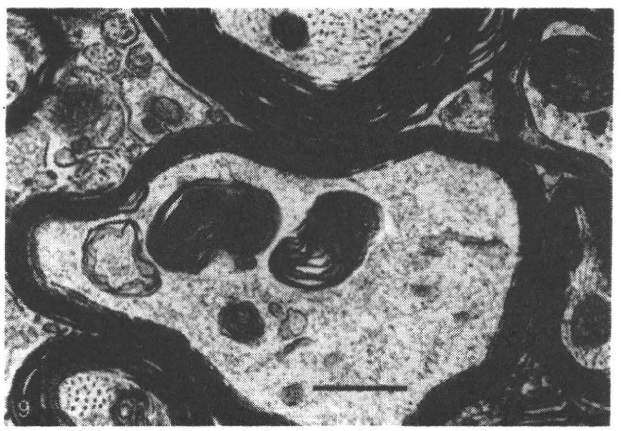

FIGURE 9. Transgenic mouse (24 weeks). The mitochondria in these axons appear as electron-dense membranous or amorphous structures. Scale bar = 0.5 μm.

FIGURE 11. Transgenic mouse (24 weeks). Electron-dense multiply folded membranes of the cristae in a dendrite mitochondrion. Scale bar = 0.5 μm.

FIGURE 12. Transgenic mouse (24 weeks). Outward projection of inner and outer membranes of a mitochondrion is observed in a presynaptic bouton. Scale bar = 0.5 μm.

Immunoelectron Microscopic Findings

To determine the ultrastructural distribution of human SOD1 and ubiquitin immunoreactivity, we used postembedding immunogold electron microscopy. Abundant human SOD1 and ubiquitin immunogold labeling was observed in the profiles of small to large aggregates (Fig. 14) even in samples obtained at the preclinical stage. Cu/Zn superoxide dismutase and ubiquitin determinants were undetectable in both most normal-appearing mitochondria (Fig. 14) and in degenerated or abnormal mitochondria (Fig. 15), although rare mitochondria showed SOD1-immunogold labeling (Fig. 16).

No phosphorylated neurofilament immunogold labeling was detected in the aggregates, LIs, or the mitochondria. No control mice at any age showed SOD1- or ubiquitin-positive aggregates, LIs, or cord-like axonal swelling.

DISCUSSION

Accumulating evidence strongly suggests that mitochondrial dysfunction plays a role in the pathogenetic mechanisms of motor neuron degeneration in ALS (5–10). Functional abnormalities including elevated levels of mutant mitochondrial DNA in the spinal cord (7) and the motor cortex (9), reduced mitochondrial DNA in the spinal cord (7), changes in the activity of complex I of the mitochondria respiratory chain in familial ALS patients (8, 12), decreased complex IV activity in the spinal motor neurons of sporadic ALS patients (13, 14), and the possible involvement of some mitochondrial haplotype variations in the risk of ALS development (15) have been reported. An out-of-frame mutation of mitochondrial DNA encoding subunit I of cytochrome *c* oxidase in a patient with motor neuron disease has also been reported (16). Mitochondrial dysfunction can lead to increased cytosolic calcium levels as a result of cellular depolarization (17) which would most likely result in motor neuron death, because large motor neurons do not contain calcium-binding proteins such as parvalbumin and calbindin D-28k and are less able to buffer calcium (18). Moreover, the vulnerability of motor neurons to excitotoxicity is selectively enhanced when mitochondrial function is impaired (19).

There have been several observations of morphological mitochondrial abnormalities in sporadic ALS patients. These include bizarre giant mitochondria in liver biopsy specimens (20, 21), abnormal accumulation of mitochondria in the axon hillock and the initial segment of axons (22), conglomeration of dark abnormal mitochondria at the presynaptic terminals of anterior horn neurons (5), and mitochondria with increased volumes in muscle biopsies (6). We recently reported several morphological changes in the mitochondria in the somata of the anterior horn neurons and neuronal processes in patients with sporadic ALS, including a stack of multilayered, linear cristae in the mitochondria in the somata of anterior horn neurons and their axons (23), swollen mitochondria with markedly increased cristae in the somata of the anterior horn neurons (23), and increased numbers of unusual inclusion bodies consisting of tubular structures of the mitochondrial cristae in the somata of dorsal root ganglion cells in sporadic ALS patients (24). The morphological changes in the mitochondria of H46R mutant SOD1 Tg mice are, however, quite different from those in sporadic ALS (23, 24), but markedly swollen mitochondria with increased numbers of cristae have been seen in both diseases.

There is also accumulating evidence that mitochondria are a major target of mutant SOD1 toxicity. In mice possessing high copy numbers of the G93A transgene and G37R mutant SOD1, both mitochondrial swelling and vacuolation begin at early stages of disease (11, 25) and peak at the onset of muscle weakness (10). In cultured neuroblastoma cells or motor neurons, the expression of mutant SOD1 causes mitochondrial damage and dysfunction (26, 27). Furthermore, various mitochondrial electron transport chain activities are decreased in the anterior horn before the disease onset and during the stage of disease progression (28). Thus, mitochondrial abnormalities may play an early role in pathways leading to cell death, or may occur as a consequence of other subtle impairments and contribute to mechanisms of chronic neurodegeneration (29).

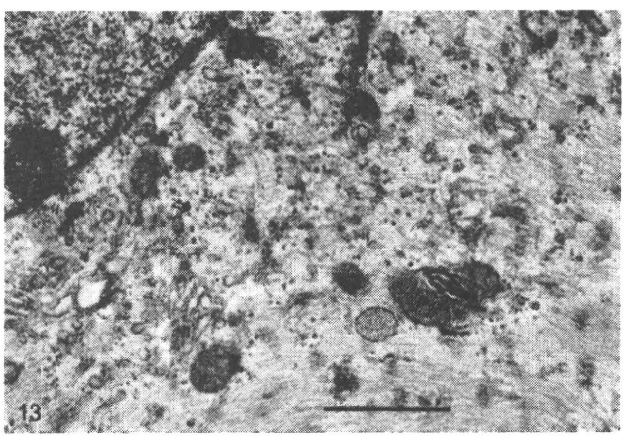

FIGURE 13. Transgenic mouse (24 weeks). An astrocyte contains cytoplasmic glial fibrils and an abnormal mitochondrion with electron-dense changes of the cristae. Scale bar = 1 μm.

TABLE. Semiquantitative Analysis of the Incidence of Abnormal Mitochondria in the Spinal Cord Anterior Column of Transgenic Mice

Age, weeks	Total Number of Mitochondria Examined	Electron-Dense Alterations in the Cristae	%	Number of Whorled Membranous Structures	%	Outward Projection of the Inner and Outer Membranes	%
12	2,612	5	0.19	19	0.73	0	0.00
16	2,611	4	0.15	41	1.57	5	0.19
20	1,880	60	3.19	44	2.34	17	0.90
24	1,666	158	9.48	61	3.66	5	0.30
Fisher exact test (p value)							
12-week vs 16-week		1.000		0.004		0.031	
12-week vs 20-week		<0.001		<0.001		<0.001	
12-week vs 24-week		<0.001		<0.001		0.009	

In this study, we demonstrated that all components of the mitochondria in the spinal cords of H46R mutant SOD1 Tg mice are altered. In particular, electron-dense changes of cristae were intriguing findings that were predominantly recognized in axons starting at the preclinical stage and progressing later through the overt clinical stage. These alterations were subsequently also observed in the somata, dendrites, presynaptic terminals, and astrocyte cytoplasm at the later stages. The alterations in the cristae may reflect a disturbance in energy generation related to enzymes of the respiratory electron–transport chain that are attached to the cristae and project into the matrix. Furthermore, outer mitochondrial membrane damage probably results in membrane permeabilization, which is lethal because it triggers the release of caspase-activating molecules and caspase-independent death effectors, metabolic failure in the mitochondria, or both (30). Thus, these structural changes in the mitochondria may reflect mitochondrial dysfunction in the motor neurons and be related to the neurodegeneration in these mutant mice. These electron-dense alterations of cristae are characteristic of these H46R SOD1 Tg mice and contrast to the vacuolar changes predominant in Tg mice that express high levels of G93A mutant SOD1 (10, 25, 31–33) and G37R mutant SOD1 (11). On the other hand, G93A mutant SOD1 Tg mice with a low transgene copy number (34) and G85R mutant SOD1 Tg mice (35) showed no vacuoles, which is also the case in H46R mutant SOD1 Tg mice. These findings suggest that the mitochondria may undergo morphologically protean alterations according to differences in SOD1 mutations, different levels of SOD1 toxicity, and at different disease stages. The predominance of these mitochondrial abnormalities in the proximal axons even at preclinical stage observed in this study implies a disruption of axonal transport of the substrates needed for neuronal viability starting at the preclinical stage that eventually leads to motor neuron degeneration. Predominant abnormalities of the mitochondria in the proximal axons are also reminiscent of those in Tg mice, with a relatively low transgene copy number expressing a G93A mutant human SOD1; these latter mice predominantly exhibit vacuoles in the mitochondria of the axons but not in the somata of anterior horn cells or in their dendrites at any stage of disease (31).

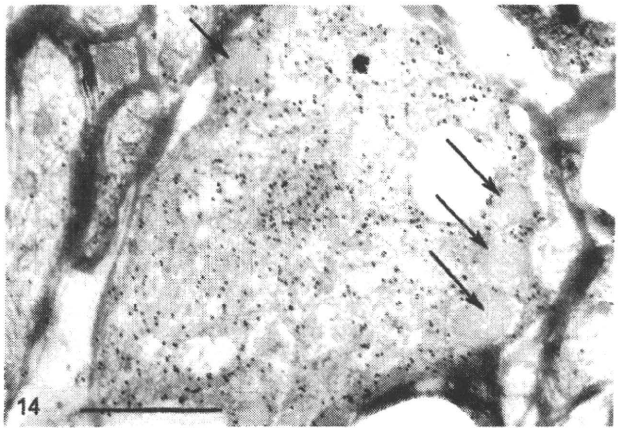

FIGURE 14. Transgenic mouse (20 weeks). Cu/Zn superoxide dismutase (SOD1) determinants are not present in the inner compartments of normal-appearing mitochondria (arrows) at the periphery of the aggregate, which shows a high level of human SOD1-immunogold labeling. Scale bar = 1 μm.

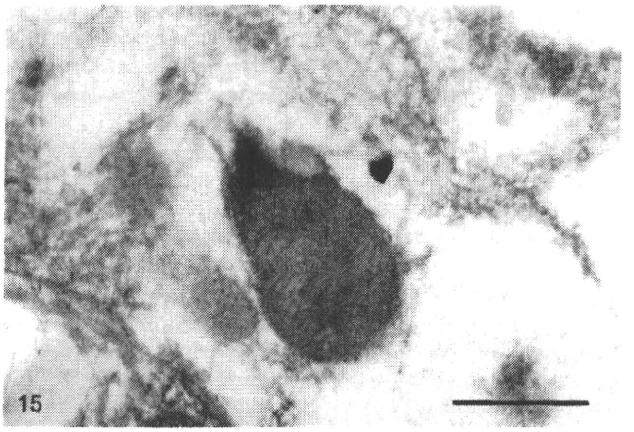

FIGURE 15. Transgenic mouse (20 weeks). No increase in human Cu/Zn superoxide dismutase–immunogold labeling is observed in a degenerated or abnormal mitochondrion. Scale bar = 0.5 μm.

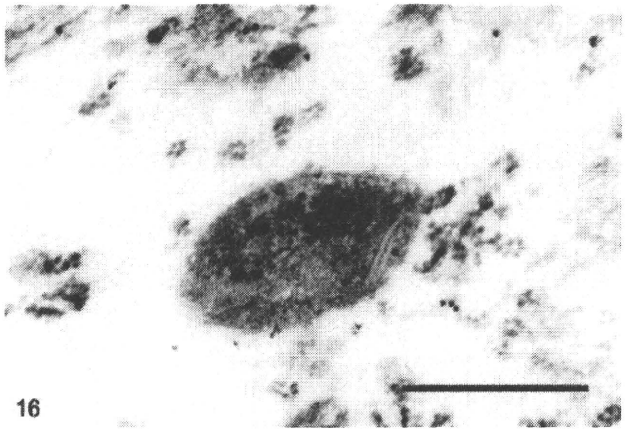

FIGURE 16. Transgenic mouse (20 weeks). Only occasional mitochondria show an increase in Cu/Zn superoxide dismutase–immunogold labeling. Scale bar = 0.5 μm.

Our present finding that mitochondrial alterations exhibited in the anterior horn neurons and neuronal processes are also observed in astrocyte cytoplasm at the overt clinical stage in this study is also intriguing. Similar mitochondrial alterations have not been detected in the astrocytes of G93A mutant SOD1 Tg mice (31), whereas accumulating evidence suggests that non-neuronal cells such as astrocytes might directly contribute to the neuronal loss and have prominent roles in the neurodegenerative disorders that are often characterized by distinctive local astrocytosis (36). One of the potential candidates for pathogenic mechanisms in ALS has also been linked to neuronal excitotoxicity from excessive extracellular glutamate due to the dysfunction of astrocytic glutamate transporters (37). Toxicity to motor neurons is known to be noncell autonomous because wild-type non-neuronal cells can delay or eliminate degeneration and death of SOD1 mutant-expressing motor neurons and wild-type neurons acquiring damage from mutant-expressing neighbors (38). Thus, our findings of mitochondrial abnormalities in astrocytes suggest that impairment of astrocytes may also influence motor neuron degeneration or death.

Some immunoelectron-microscopic studies have indicated that SOD1 is distributed throughout the cytoplasm, in the nucleus, and in peroxisomes but not in the mitochondria (39, 40), whereas other studies indicate that SOD1 is present inside mitochondria (28, 41–43) and that mutant SOD1 is associated with abnormal mitochondria in the central nervous system of mice (32, 44). In G93A mutant Tg mice and mice-expressing wild-type human SOD1, far more SOD1-immunogold particles are present in the mitochondria than in the mitochondria of their non-Tg littermates (31, 33, 41), suggesting that the altered mitochondria of Tg mice are closely associated with SOD1-induced motor neuron degeneration. In the present study, SOD1-immunogold particles were not observed either in normal-appearing or abnormal mitochondria, which suggests that SOD1-induced neurotoxicity may not be directly related to mitochondrial degeneration, but that mitochondrial alterations may be secondarily caused by the mutation in H46R mutant SOD1 Tg mice.

Mitochondria are known to play complex roles in the pathogenesis of neurodegenerative diseases due to their involvement in the regulation of excitotoxicity, the homeostasis of intracellular Ca^{2+}, reactive oxygen species production, and apoptotic processes. The significance of the mitochondrial abnormalities observed here and their connection with oxidative stress, excitotoxicity, and mitochondrial apoptosis in H46R mutant SOD1 Tg mice remains to be elucidated. The demonstration of mitochondrial damage in H46R mutant SOD1 Tg mice, whether these abnormalities are primary or secondary, suggests that therapeutic compounds capable of modulating or rescuing mitochondrial function may exert a protective function or even prevent the degeneration of motor neurons.

ACKNOWLEDGMENT

The authors wish to thank Dr Y. Horie (Division of Biostatistics, Kitasato University Graduate School, Tokyo) for statistical analysis.

REFERENCES

1. Aoki M, Ogasawara M, Matsubara Y, et al. Familial amyotrophic lateral sclerosis (ALS) in Japan associated with H46R mutation in Cu/Zn superoxide dismutase gene: A possible new subtype of familial ALS. J Neurol Sci 1994;126:77–83
2. Ohi T, Saita K, Takechi S, et al. Clinical features and neuropathological findings of familial amyotrophic lateral sclerosis with a His 46Arg mutation in Cu/Zn superoxide dismutase. J Neurol Sci 2002;197:73–78
3. Arisato T, Okubo R, Arata H, et al. Clinical and pathological studies of familial amyotrophic lateral sclerosis (FALS) with SOD1 H46R mutation in large Japanese families. Acta Neuropathol 2003;106:561–68
4. Sasaki S, Nagai M, Aoki M, Komori T, Itoyama Y, Iwata M. Motor neuron disease in transgenic mice with an H46R mutant SOD1 gene. J Neuropathol Exp Neurol 2007;66:517–24
5. Sasaki S, Iwata M. Ultrastructural study of synapses in the anterior horn neurons of patients with amyotrophic lateral sclerosis. Neurosci Lett 1996;204:53–56
6. Siklos L, Engelhardt J, Harati Y, Smith RG, Joo F, Appel SH. Ultrastructural evidence for altered calcium in motor nerve terminals in amyotrophic lateral sclerosis. Ann Neurol 1996;39:203–16
7. Wiedemann FR, Manfredi G, Mawrin C, Beal MF, Schon EA. Mitochondrial DNA and respiratory chain function in spinal cords of ALS patients. J Neurochem 2002;80:616–25
8. Bowling AC, Schulz JB, Brown RH, Beal MF. SOD activity, oxidative damage, and mitochondrial energy metabolism in familial and sporadic ALS. J Neurochem 1993;61:2322–25
9. Dhaliwal GK, Grewall RP. Mitochondrial DNA deletion mutation levels are elevated in ALS brains. Neuroreport 2000;11:2507–9
10. Kong J, Xu Z. Massive mitochondrial degeneration in motor neurons triggers the onset of amyotrophic lateral sclerosis in mice expressing a mutant SOD1. J Neurosci 1998;18:3241–50
11. Wong PC, Pardo CA, Borchelt DR, et al. An adverse property of a familial ALS-linked SOD1 mutation causes motor neuron disease characterized by vacuolar degeneration of mitochondria. Neuron 1995;14:1105–16
12. Browne SE, Bowling AC, Baik MJ, Gurney M, Brown RH Jr, Beal MF. Metabolic dysfunction in familial, but not sporadic, amyotrophic lateral sclerosis. J Neurochem 1998;71:281–87
13. Fujita K, Yamauchi M, Shibayama K, Ando M, Honda M, Nagata Y. Decreased cytochrome c oxidase activity but unchanged superoxide dismutase and glutathione peroxidase activities in the spinal cords of patients with amyotrophic lateral sclerosis. J Neurosci Res 1996;45:276–81
14. Borthwick GM, Johnson MA, Ince PG, Shaw PJ, Turnbull DM. Mitochondrial enzyme activity in amyotrophic lateral sclerosis: Implications for the role of mitochondria in neuronal cell death. Ann Neurol 1999;46:787–90

15. Mancuso M, Conforti FL, Rocchi A, et al. Could mitochondrial haplogroups play a role in sporadic amyotrophic lateral sclerosis? Neurosci Lett 2004;371:158–62
16. Comi GP, Bordoni A, Salani S, et al. Cytochrome *c* oxidase subunit I microdeletion in a patient with motor neuron disease. Ann Neurol 1998;43:110–16
17. McLaughlin BA, Nelson D, Silver IA, Erecinska M, Chesselet MF. Methylmalonate toxicity in primary neuronal cultures. Neuroscience 1998;86:279–90
18. Ince P, Stout N, Shaw P, et al. Parvalbumin and calbindin D-28k in the human motor system and in motor neuron disease. Neuropathol Appl Neurobiol 1993;19:291–99
19. Kaal EC, Vlug AS, Versleijen MW, Kuilman M, Joosten EA, Bar PR. Chronic mitochondrial inhibition induces selective motoneuron death in vitro: A new model for amyotrophic lateral sclerosis. J Neurochem 2000; 74:1158–65
20. Matsui Y, Mozai T, Kakehi K. Functional and morphometric study of the liver in motor neuron disease. J Neurol 1985;232:15–19
21. Nakano K, Hirayama K, Terao K. Hepatic ultrastructural changes and liver dysfunction in amyotrophic lateral sclerosis. Arch Neurol 1987;44: 103–6
22. Sasaki S, Iwata M. Impairment of fast axonal transport in the proximal axons of anterior horn neurons in amyotrophic lateral sclerosis. Neurology 1996;47:535–40
23. Sasaki S, Iwata M. Mitochondrial alterations in the spinal cord of patients with sporadic amyotrophic lateral sclerosis. J Neuropathol Exp Neurol 2007;66:10–16
24. Sasaki S, Horie Y, Iwata M. Mitochondrial alterations in dorsal root ganglion cells in sporadic amyotrophic lateral sclerosis. Acta Neuropathol 2007;114:633–39
25. Dal Canto MC, Gurney ME. Neuropathological changes in two lines of mice carrying a transgene for mutant human Cu, Zn SOD, and in mice overexpressing wild-type human SOD: A model of familial amyotrophic lateral sclerosis (FALS). Brain Res 1995;676:25–40
26. Carri MT, Ferri A, Battistoni A, et al. Expression of a Cu, Zn superoxide dismutase typical of familial amyotrophic lateral sclerosis induces mitochondrial alteration and increase of cytosolic Ca^{2+} concentration in transfected neuroblastoma SH-Sy5Y cells. FEBS Lett 1997;414:365–68
27. Jung C, Higgins CMJ, Xu Z. Mitochondrial electron transport chain complex dysfunction in a transgenic mouse model for amyotrophic lateral sclerosis. J Neurochem 2002;3;535–45
28. Okado-Matsumoto A, Fridovich I. Subcellular distribution of superoxide dismutase (SOD) in rat liver: Cu, Zn-SOD in mitochondria. J Biol Chem 2001;276:38388–93
29. Curti D, Malaspina A, Facchetti G, et al. Amyotrophic lateral sclerosis: Oxidative energy metabolism and calcium homeostasis in peripheral blood lymphocytes. Neurology 1996;47:1060–64
30. Green DR, Kroemer G. The pathophysiology of mitochondrial cell death. Science 2004;305:626–29
31. Sasaki S, Warita H, Murakami T, Abe K, Iwata M. Ultrastructural study of mitochondria in the spinal cord of transgenic mice with a G93A mutant SOD1 gene. Acta Neuropathol (Berl) 2004;107:461–74
32. Dal Canto MC, Gurney ME. Development of central nervous system pathology in a murine transgenic model of human amyotrophic lateral sclerosis. Am J Pathol 1994;145:1271–79
33. Jaarsma D, Rognoni F, van Duijn W, Verspaget HW, Haasdijk ED, Holstege JC. CuZn superoxide dismutase (SOD1) accumulates in vacuolated mitochondria in transgenic mice expressing amyotrophic lateral sclerosis-linked SOD1 mutations. Acta Neuropathol (Berl) 2001;102: 293–305
34. Dal Canto MC, Gurney ME. A low expressor line of transgenic mice carrying a mutant human Cu,Zn superoxide dismutase (SOD1) gene develops pathological changes that most closely resemble those in human amyotrophic lateral sclerosis. Acta Neuropathol (Berl) 1997;93: 537–50
35. Bruijn LI, Becher MW, Lee MK, et al. ALS-linked SOD1 mutant G85R mediates damage to astrocytes and promotes rapidly progressive disease with SOD1-containing inclusions. Neuron 1997;18:327–38
36. Lobsiger CS, Cleveland DW. Glial cells as intrinsic components of non-cell-autonomous neurodegenerative disease. Nat Neurosci 2007;10: 1355–60
37. Rothstein JD, Van Kammen M, Levey AI, Martin LJ, Kuncl RW. Selective loss of glial glutamate transporter GLT-1 amyotrophic lateral sclerosis. Ann Neurol 1995;38:73–84
38. Clement AM, Nguyen MD, Roberts EA, et al. Wild-type nonneuronal cells extend survival of SOD1 mutant motor neurons in ALS mice. Science 2003;302:113–17
39. Crapo JD, Oury T, Rabouille C, Slot JW, Chang LY. Copper, zinc superoxide dismutase is primarily a cytosolic protein in human cells. Proc Natl Acad Sci U S A 1992;89:10405–9
40. Slot JW, Geuze HJ, Freeman BA, Crapo JD. Intracellular localization of the copper-zinc and manganese superoxide dismutases in rat liver parenchymal cells. Lab Invest 1986;55:363–71
41. Higgins CM, Jung C, Ding H, Xu Z. Mutant Cu, Zn superoxide dismutase that causes motoneuron degeneration is present in mitochondria in the CNS. J Neurosci 2002;22:RC215
42. Sturtz LA, Diekert K, Jensen LT, Lill R, Culotta VC. A fraction of yeast Cu, Zn-superoxide dismutase and its metallochaperone, CCS, localize to the intermembrane space of mitochondria. A physiological role for SOD1 in guarding against mitochondrial oxidative damage. J Biol Chem 2001; 276:38084–89
43. Weisiger RA, Fridovich I. Mitochondrial superoxide dismutase. Site of synthesis and intramitochondrial localization. J Biol Chem 1973;248: 4793–96
44. Levine JB, Kong J, Nadler M, Zu Z. Astrocytes interact intimately with degenerating motor neurons in mouse amyotrophic lateral sclerosis (ALS). Glia 1999;28:215–24

Chromogranin B P413L variant as risk factor and modifier of disease onset for amyotrophic lateral sclerosis

Francois Gros-Louis[a], Peter M. Andersen[b], Nicolas Dupre[c], Makoto Urushitani[d], Patrick Dion[e], Frederique Souchon[f], Monique D'Amour[f], William Camu[g], Vincent Meininger[h], Jean-Pierre Bouchard[c], Guy A. Rouleau[e], and Jean-Pierre Julien[a,1]

[a]Centre de Recherche du Centre Hospitalier Universitaire de Québec, Département de psychiatrie et neurosciences, Université Laval, Ste-Foy, QC, Canada G1V 4G2; [b]Institute of Clinical Neuroscience, Umeå University Hospital, SE-901 85 Umeå, Sweden; [c]Faculty of Medecine, Laval University, Department of Neurological Sciences, Enfant-Jesus Hospital, Quebec City, QC, Canada G1J 1Z4; [d]Molecular Neuroscience Research Center, Shiga University of Medical Science, Seta-Tsukinowa-cho, Otsu, Shiga 520-2192, Japan; [e]Center for Excellence in Neuromics, Centre Hospitalier de l'Université de Montréal Research Center–Notre Dame Hospital, and University of Montreal, QC, Canada H2L 2W5; [f]Centre Hospitalier de l'Université de Montréal, Department of Neurology, Notre-Dame Hospital, QC, Canada H2L 4M1; [g]Unité de Neurologie Comportementale et Dégénérative, Institute of Biology, Montpellier 34967, France; and [h]Fédération des Maladies du Système Nerveux, Division Paul Castaigne, Hôpital de la Salpêtrière, Paris 75651, France

Edited by Robert H. Brown, Jr., University of Massachusetts Medical School, and accepted by the Editorial Board October 27, 2009 (received for review February 27, 2009)

Recently, chromogranins were reported to interact specifically with mutant forms of superoxide dismutase that are linked to amyotrophic lateral sclerosis (ALS). This interaction led us to analyze the frequencies of sequence variants of the *CHGB* gene in ALS patients and matched controls from three different countries. Of particular interest was the finding of the P413L *CHGB* variant present in 10% of ALS patients ($n = 705$) as compared to 4.5% in controls ($n = 751$), conferring a 2.2-fold greater relative risk to develop the disease ($P < 0.0001$). This effect was mainly contributed by the samples of French origin that yielded a frequency of the P413L variation at 17% in ALS ($n = 289$) and 5% in controls ($n = 448$), conferring a 3.3-fold greater risk to develop ALS. Furthermore, the P413L *CHGB* variant is associated with an earlier age of onset by almost a decade in both sporadic ALS and familial ALS cases. Genetic variation influencing age of onset in ALS had not previously been reported. Expression of fusion CHGB-EGFP constructs in SHSY-5Y cells revealed that the P413L variation can cause defective sorting of CHGB into secretory granules. The finding that *CHGB* may act as a susceptibility gene and modifier of onset in ALS is consistent with the emerging view that dysfunction of the secretory pathway may contribute to increased vulnerability of motor neurons.

association study | modifier gene | motor neuron

Amyotrophic lateral sclerosis (ALS) is the most common adult-onset neurodegenerative disorder characterized by the death of large motor neurons in the cerebral cortex and spinal cord (1). Although most cases of ALS are sporadic (SALS), some families demonstrate a clinically indistinguishable form of ALS with clear Mendelian inheritance and high penetrance (familial ALS or FALS) (2). Despite many years of intensive study, very few genes have been unequivocally implicated in ALS, including the well-known superoxide dismutase 1 (*SOD1*) gene, which accounts for about 2 to 5% of all ALS cases (3, 4). The mechanism whereby mutant *SOD1* causes specific degeneration of motor neurons remains unclear, but it is believe that disease is caused by a gain of a toxic function of mutant SOD1 protein (5–7). Recently, a specific interaction between chromogranins and different mutant forms of SOD1 led to a new ALS pathogenic model based on chromogranin-mediated secretion of toxic mutant SOD1 molecules (8). Chromogranins can also interact with oxidized WT SOD1 but not with intact WT SOD1 (9). This interaction is further supported by the recent report of a colocalization of chromogranins with SOD1-immunopositive aggregates in motor neurons of sporadic ALS cases (10). Moreover, there is evidence of altered chromogranin expression in the saliva of ALS patients (11). These combined observations led us to screen the *CHGB* gene for sequence variations in sporadic and familial ALS patients from France, Canada (French Canadian origin), and Sweden.

Results

***CHGB* Variations Identified in ALS Patients from France and Canada/Quebec.** We initially screened the *CHGB* gene for sequence variations in the entire ORF and the flanking intron/exon borders in 194 individuals, of French or French Canadian origin, with either familial or sporadic ALS and 258 healthy controls of similar age, geography, and ethnicity (Table 1). A total of 21 single nucleotide variations were detected in the *CHGB* gene, including eight previously unrecorded sequence variations that were not present in the SNP database (Table 2). Fifteen of these 21 sequence variations occurred within coding regions, five were found within introns, and one in the 3′ untranslated region of the gene. Interestingly, all of the coding variations were located in exon 4 and 11 of them led to amino acid changes. Two different bioinformatics protein prediction software (PolyPhen and Pmut) were used to assess whether the 11 missense variations are potentially pathological or lead to protein structure defect (Table S1). Among these 11 nonsynonymous variations, three (R101K, H230R, and R258Q) were not found in 516 control chromosomes. The R101K variation leading to a conservative amino acid change was present in only one ALS patient. The patient had no familial history of neurological disorder and he first presented classic ALS symptoms in the lower-limb at the age of 42 years. The H230R missense variation is predicted to have a functional effect on protein structure (Polyphen: probably damaging, Position-Specific Independent Count or PSIC score of 2.696) and likely a pathological effect (Pmut: prediction score of 0.5510) according to the protein-prediction software. This variation was found in one FALS patient and in one SALS patient, but was absent in control individuals. The non-SOD1

Author contributions: F.G.-L., P.D., G.A.R., and J.-P.J. designed research; F.G.-L. and M.U. performed research; P.M.A., N.D., F.S., M.D., W.C., V.M., J.-P.B., and G.A.R. contributed new reagents/analytic tools; F.G.-L. and J.-P.J. analyzed data; and F.G.-L. and J.-P.J. wrote the paper.

The authors declare no conflict of interest.

This article is a PNAS Direct Submission. R.H.B. is a guest editor invited by the Editorial Board.

[1]To whom correspondence should be addressed at: 2705 Boulevard Laurier (Bloc T2), Ste-Foy, Quebec, Canada, G1V 4G2. Email: jean-pierre.julien@crchul.ulaval.ca.

This article contains supporting information online at www.pnas.org/cgi/content/full/0902174106/DCSupplemental.

Table 1. Clinical details of study populations

Study population	FALS-non SOD1	FALS-SOD1	SALS	Controls
French (France and Canada/Quebec)				
Number of individuals	40	0	249	448
Mean age of onset, years (range)	55 (35–64)	NA	58 (23–82)	60* (34–93)
Disease duration, years (±SE)	4.1 ± 0.7	NA	4.3 ± 0.4	NA
Males	21	NA	155	167
Females	19	NA	94	281
Swedish				
Number of individuals	61	40	315	303
Mean age of onset, years (range)	57 (35–78)	49 (29–77)	60 (20–89)	62* (25–94)
Disease duration, years (±SE)	4.7 ± 0.8	11.3 ± 2.1	3.0 ± 0.2	NA
Males	30	23	178	158
Females	31	17	137	145
Total				
Number of individuals	101	40	564	751
Mean age of onset, years (range)	56 (35–78)	49 (29–77)	59 (20–87)	62* (25–94)
Disease duration, years (±SE)	4.4 ± 0.5	11.3 ± 2.1	3.4 ± 0.2	NA
Males	51	23	333	325
Females	50	17	231	426

NA, not applicable.
*Mean age at DNA sampling.

FALS patient first presented with classic ALS in the upper-limb at the age of 56 years. She had another affected brother who had died of ALS at the age of 83 years and, unfortunately, no DNA was available to confirm whether the affected brother was also carrying the variation. No clinical information was available for the SALS patient. The R258Q found in two different FALS cases represents a nonconserved amino acid change leading to the substitution of a polar amino acid for a polar uncharged amino acid. Unfortunately, no additional family members from the two French families were available for further study. The synonymous E169E silent variation was found in two ALS patients and not found in controls.

Of particular interest was the finding of a common variant (P413L) that was significantly increased in ALS patient chromosomes when compared to the control population ($P < 0.0001$). This variation is predicted to have a functional effect and to alter the protein structure (Polyphen: possibly damaging, PSIC score of 1.741) and also to have a pathological effect (Pmut: prediction score of 0.8075). To explore the significance of the association of the P413L variant with ALS, we screened

Table 2. Details, location, and genomic context of each sequence variants within *CHGB* genes found in ALS patients and control chromosomes in the initial screen (French and French Canadians)

Variant*	dbSNP	Intron/Exon	Amino acid change	Frequency (%)			*P* value		
				FALS	SALS	Ctrl	FALS	SALS	Combined
g.5082G>A	rs236146	Intron 2	NA	17/80 (21.3)	19/116 (16.4)	28/190 (14.7)	0.190	0.699	0.338
g.10573C>A	rs4815876	Intron 3	NA	29/80 (36.3)	34/116 (29.3)	56/190 (29.5)	0.274	0.976	0.570
g.10602A>T		Intron 3	NA	0/80 (0)	1/116 (0.9)	0/516 (0)	NA	0.035	0.104
g.10651G>T		Intron 3	NA	0/80 (0)	1/116 (0.9)	0/516 (0)	NA	0.035	0.104
g.10787T>A	s6085324	Exon 4	S93T	8/80 (22.5)	23/116 (19,8)	69/326 (21,2)	0.794	0.760	0.947
g.10812G>A		**Exon 4**	**R101K**	**0/80 (0)**	**1/116 (0.9)**	**0/516 (0)**	**NA**	**0.035**	**0.104**
g.10912G>C		Exon 4	A134A	1/80 (1.3)	1/116 (0.9)	22/326 (6.7)	0.057	0.014	0.002
g.11017G>A		**Exon 4**	**E169E**	**1/80 (1.3)**	**1/116 (0.9)**	**0/516 (0)**	**0.011**	**0.035**	**0.022**
g.11043G>A	rs910122	Exon 4	R178Q	32/80 (40)	34/116 (29.3)	110/326 (33.7)	0.293	0.382	0.987
g.11108A>C	rs881118	Exon 4	N200H	4/80 (5)	3/116 (2.6)	14/326 (4.3)	0.784	0.411	0.684
g.11199A>G		**Exon 4**	**H230R**	**1/80 (1.3)**	**1/116 (0.9)**	**0/516 (0)**	**0.011**	**0.035**	**0.022**
g.11237A>G	rs236151	Exon 4	T243A	67/80 (83.8)	88/116 (75.9)	141/190 (74.2)	0.089	0.747	0.258
g.11283G>A		**Exon 4**	**R258Q**	**2/80 (2.5)**	**0/116 (0)**	**0/516 (0)**	**≤0.0001**	**NA**	**0.022**
g.11568C>G	rs236152	Exon 4	A353G	31/80 (38.8)	36/116 (31)	60/190 (31.6)	0.255	0.921	0.586
g.11614A>G	rs236153	Exon 4	E368E	31/80 (38.8)	36/116 (31)	60/190 (31.6)	0.255	0.921	0.586
g.11652G>T		Exon 4	W381L	1/80 (1.3)	0/116 (0)	1/326 (0.3)	0.280	0.550	0.716
g.11748C>T	**rs742710**	**Exon 4**	**P413L**	**8/80 (10)**	**40/482 (8.3)**	**20/760 (2.6)**	**≤0.0001**	**≤0.0001**	**≤0.0001**
g.11760G>A	rs742711	Exon 4	R417Q	15/80 (18.8)	19/116 (16.4)	42/190 (22,1)	0.537	0.224	0.240
g.12463C>T		Exon 4	D651D	0/80 (0)	2/116 (1.7)	1/516 (0,2)	0.694	0.030	0.128
g.13270G>A	rs236155	Intron 4	NA	29/80 (36.3)	30/116 (25.9)	60/190 (31,6)	0.456	0.287	0.753
g.13499C>A	rs2821	3'UTR	NA	29/80 (36.3)	48/116 (41.4)	78/190 (41,1)	0.461	0.955	0.723

The entire open reading frame and the flanking intron/exon borders were covered by our analysis. Frequency calculation was done using the total number of chromosomes. Coding sequence variations found exclusively in patients or overrepresented in ALS patients are in boldface. NA, not applicable.
*Variants were named according to *CHGB* genomic sequence NM_001819; The nucleotide "A" of the ATG initiation codon is referred as 1.

Table 3. Validation of selected *CHGB* variants in the Swedish population

CHGB variant	Frequency (%)			*P*-value		
	FALS	SALS	Ctrl	FALS	SALS	Combined
R101K	0/202 (0)	0/630 (0)	0/606 (0)	NA	NA	NA
E169E	0/202 (0)	0/630 (0)	0/606 (0)	NA	NA	NA
H230R	1/202 (0.5)	2/630 (0.3)	1/606 (0.1)	0.414	0.586	0.487
R258Q	1/202 (0.5)	0/630 (0)	0/606 (0)	0.083	NA	0.393
P413L	6/202 (3.0)	16/630 (2.6)	11/606 (1.8)	0.084	0.385	0.300

Frequencies have been calculated using total number of chromosomes for each patients and controls. NA, not applicable.

95 additional SALS patients and 190 additional nonneurological healthy individuals for this particular variant. Overall, the frequency of this particular SNP was of 17% in ALS patients as compared to 5% in controls [odds ratio (OR) of 3.7 with 95% confidence interval (CI) of 2.2–6.4], conferring a relative risk of 3.3 times greater to develop disease.

Replication and Validation of our Initial Screen in the Swedish Population. To validate our initial results with the French and French Canadian population, we further investigated the occurrence of the R101K, E169E, H230R, R258Q, and P413L sequence variations in the Swedish population (Table 3). The R101K substitution, previously found in one French Canadian SALS case, was not detected in either 832 patient chromosomes or 606 control chromosomes from Sweden. The H230R substitution was initially found in one FALS case from France and one French Canadian SALS patient. It was also present in two other SALS cases from Sweden, one FALS case homozygous for the D90A *SOD1* mutation, and one Swedish control individual. The first SALS patient from Sweden carrying the H230R variation suffered from a sporadic progressive bulbar paresis variant of ALS. He developed his first symptom at the age of 61 years. The second SALS case from Sweden with the same variation had typical leg-onset ALS, which he developed at the age of 68 years. Interestingly, this variation was also found in one FALS patient homozygous for the D90A *SOD1* mutation. The patient was a Finnish-born man with slowly progressing ALS with leg-onset at the age of 46 years. He also presented some ataxia symptoms, which is not uncommon in patients bearing the D90A *SOD1* mutation. This patient had two unaffected older brothers in their sixties, as well as an unaffected son. He therefore was the only affected individual in his family but he is considered as a familial case because of the presence of the *SOD1* mutation. Although the H230R variant was also found in one control individual from Sweden, an increased allele frequency is still observed for the substitution in total ALS cases we examined (OR 5.5; 95% CI of 0.6–47.3) (Table 4). The R258Q substitution, found initially in two French FALS cases, was also found in one FALS case from Sweden, and was not detected in control individuals. However, the R258Q variation is unlikely to be pathogenic, as this variation was not detected in three other affected family members from the same Swedish FALS pedigree. The E169E synonymous variation was not detected in Swedish patients or in controls. Although the frequency of the P413L variation in ALS patients from Sweden (5.2%) was not as high as in the French and French Canadian patients (17%), Swedish ALS patients carrying the P413L variation also had a greater risk for ALS (OR 1.5; 95% CI of 0.7–3.1).

Overall, the P413L (g.11748C>T) genetic variation was significantly overrepresented in ALS cases versus controls in the combined populations (OR 2.4; 95% CI 1.5–3.6), conferring a 2.2-fold greater relative risk to develop the disease ($P < 0.0001$) (see Table 4). It is noteworthy that the frequency of the "T" allele among control individuals reported here (4%) is identical to the published frequency of National Center for Biotechnology Information (NCBI) SNP database obtained from Utah individuals with Northern and Western European ancestry (for more details, see reference number "rs742710" in the NCBI SNP database).

Because the other identified genetic variations found in ALS cases are rare, it remains uncertain that they confer susceptibility to ALS. Nevertheless, when pooled together with the P413L variant, the combined *CHGB* variants significantly increased the risk of developing ALS by about 2.7 times (95% CI, 1.7–4.4), with 11.2% of total ALS patients carrying one of these variations compared to 4.1% in controls (OR 2.9; 95% CI of 1.7–4.9) (see Table 4).

***The CHGB* P413L Variant Is a Modifier of Disease Onset.** The effect of the P413L variation on the age of onset was also assessed by deriving Kaplan–Mayer curves. ALS patients carrying the P413L variant were more likely to have an earlier age of onset compared to those without this variation. SALS patients carrying the P413L variation had a median age of onset of 55 years, compared to 62 years for SALS patients without the variation ($P = 0.0001$) (Fig. 1*A*). Similarly, FALS patients with the P413L substitution

Table 4. Overall frequency of the P413L variation and cumulative proportions, odds ratios, and relative risks for identified *CHGB* variants in all combined studied populations

CHGB variants	ALS % carriers ($n = 610$)*	Ctrl % carriers ($n = 561$)*	OR (95% CI)	RR (95% CI)
P413L	10.0	3.9	2.4 (1.5–3.6)	2.2 (1.5–3.3)
R101K	0.2	0	NA	NA
E169E	0.4	0	NA	NA
H230R	1.0	0.2	5.5 (0.6–47.3)	5.5 (0.7–46.6)
R258Q	0.6	0	NA	NA
All variants	12.2	4.1	2.9 (1.7–4.9)	2.7 (1.7–4.4)

Frequencies and derived odds ratios or relative risks have been calculated using the total number of ALS patients and controls among all studied populations. OR, Odds Ratio (95% CI); RR, Relative Risk (95% CI); NA, not applicable (OR cannot be calculated because all carriers were patients thus implying a division by zero).
*Note that 705 patients and 751 matched controls have been screen for the P413L variation.

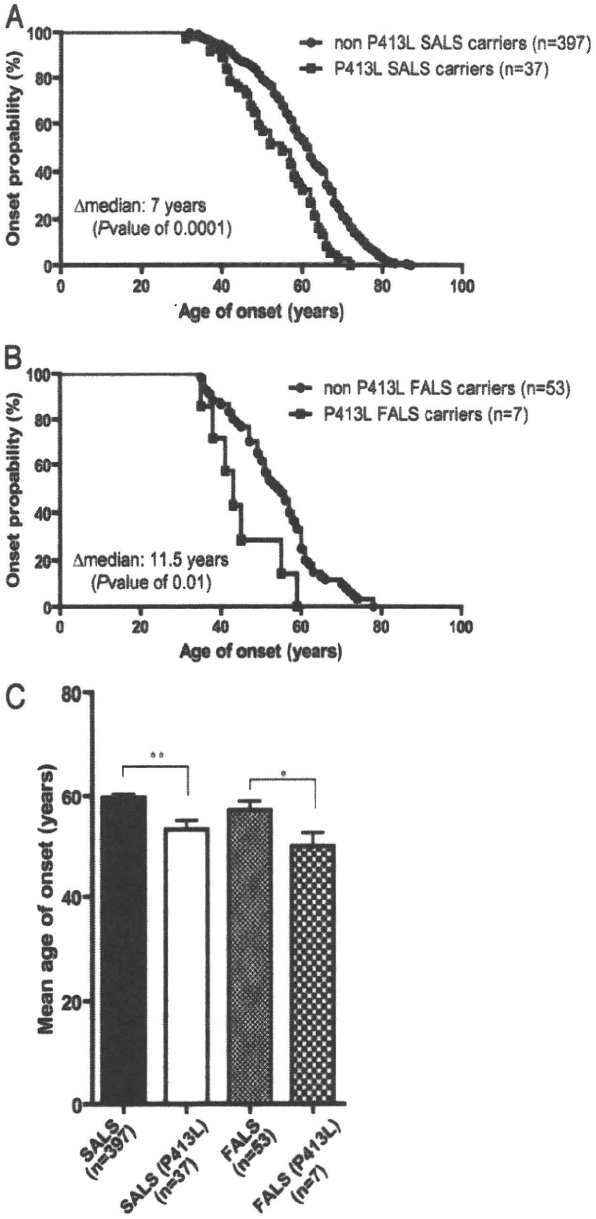

Fig. 1. Onset probability of ALS patients among carriers and noncarriers of the *CHGB* P413L variant. (*A*) The presence of the *CHGB* P413L variant among SALS patients (Median onset, 55-years) significantly reduced the age of onset (P = 0.0001) as compared to non-P413L SALS carriers (Median onset, 62-years). (*B*) The presence of the *CHGB* P413L variant among FALS carriers (Median onset, 43 years) significantly reduced the age of onset (P = 0.01) as compared to non-P413L FALS carriers (Median onset, 54.5 years). (*C*) Mean age of onset also significantly differ amongst P413L carriers vs. noncarriers among ALS patients. SALS patients carrying the P413L *CHGB* variant showed a mean age of onset of 53.3 ± 1.8 years as compared to 59.7 ± 0.7 years for noncarrier SALS patients (P = 0.008). Furthermore, FALS patients carrying the P413L *CHGB* variant also demonstrated a lower age of onset (49.8 ± 2.8 years) as compared noncarrier FALS patients (57.1 ± 1.9 years) (P = 0.05). These results strongly suggest that *CHGB* may be a modifier of the disease. The "*n*" number between brackets represents the number of patients for which we had clinical information.

had a median age of onset of 43 years compared to 55 years for FALS patients without the variation (P = 0.01) (Fig. 1*B*). The mean age of onset from patients with the P413L variation was also significantly lower when compared to patients not carrying this variation (Fig. 1*C*). SALS patients carrying the P413L variation had a mean age of onset of 53 years, compared to 60 years for SALS patients not carrying the variation (P = 0.008); the mean age of onset from FALS patients bearing the P413L variation was 50 years, compared to 57 years for FALS patients not bearing it (P = 0.05). We also investigated the cosegregation of the P413L variation in two families with other affected individuals for which DNA and clinical information were available (Table 5). The two affected individuals carrying the P413L variation from both families developed disease at the age of 45 and 41 years, as compared to 64 and 63 years for the other affected individuals not carrying the variation in their respective family. These results support the notion that the P413L variation is associated with an earlier age of onset.

Table 5. Association of the P413L variation with earlier age of onset in two different families with multiple affected individuals

Family no.	Identifier	Genotype	SOD1 mutation	Sex	Age of onset, years
ALS71	Rou7123	P413L/WT	No	M	45
ALS71	Rou7124	WT/WT	No	M	64
ALS54	Rou11348	P413L/WT	No	M	41
ALS54	Rou11353	WT/WT	No	M	63

Defective Sorting of *CHGB* Variants into Secretory Granules. To investigate the effect of the H230R and P413L *CHGB* gene variants, human neuroblastoma cells SHSY-5Y were transiently transfected with expression vectors encoding CHGB WT, CHGB H230R, or CHGB P413L variants fused to enhanced green fluorescent protein (EGFP). The subcellular localization of CHGB-EGFP protein was examined together with the Golgi-marker plasmid DsRed-Golgi, which carries the Golgi-targeting sequence of the human gene encoding 1,4-galactosyl transferase. Confocal laser microscopy revealed that after 48 h only a fraction of the WT CHGB-EGFP colocalized (about 40%) with the Golgi marker (Fig. 2). This result is consistent with the normal sorting of the protein to the secretory granules after leaving the endoplasmic reticulum (ER) transGolgi network. In contrast, the H230R and P413L CHGB-EGFP variants were almost entirely sequestered in the ER/transGolgi network (see Fig. 2), suggesting a defective sorting and maturation of these ALS-linked CHGB variants into secretory granules.

Discussion

Our results are unique in providing evidence that *CHGB* is a susceptibility gene for ALS. To assess the possible involvement of *CHGB* gene variants in ALS, we compared the allelic frequency of each variant in three different populations of ALS patients (France, Canada/Quebec, and Sweden) versus controls matched for age, sex, and ethnicity. Of particular interest is our finding of the P413L variant, which is overrepresented in ALS patients compared with age-matched controls. In these combined populations, the presence of this *CHGB* variant conferred a 2.2-times greater risk to develop ALS. For the population of French origin, the P413L variant conferred a 3.3-fold greater risk to develop ALS. The risk conferred by the P413L *CHGB* variant is quite robust when compared to other susceptibility genes reported so far (12–15). In fact, a risk factor of 3.3 is comparable to the overrepresentation by threefold of *APOE-ε4* isoform in Alzheimer's disease patients heterozygous carriers compared to aged healthy control individuals (16–18). The P413L variation is predicted to alter the protein structure and to have functional or pathological effects according to PolyPhen and Pmut protein prediction programs. Moreover, transfection studies in cultured human neuroblastoma cells showed that this sequence variation

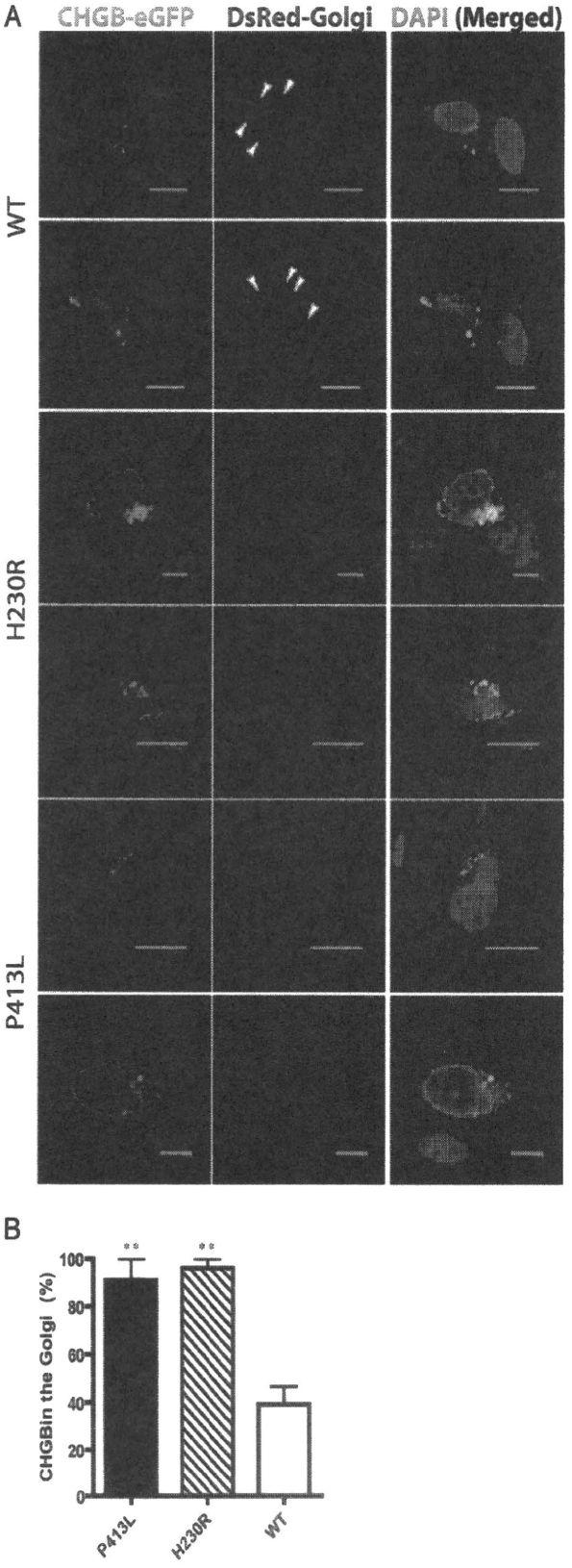

Fig. 2. Defective sorting and maturation of CHGB variants. (*A*) Confocal laser microscopy of human neuroblastoma SHSY-5Y cells that were cotransfected with EGFP-tagged human WT CHGB, H230R, or P413L CHGB variants (green) and DsRed-fused Golgi marker (*red*). After 48 h, the cells were fixed with 4% PFA and counterstained with DAPI (blue). (Scale bar, 10 μm.) (*B*) Quantification data of CHGB vesicles colocalizing with the DsRed-Golgi marker. The merged and unmerged CHGB vesicles with DsRed-Golgi marker were counted, and the percentage of CHGB in the Golgi apparatus calculated ($P = 0.009$). Note that six different cells have been counted for each conditions.

caused the abnormal sequestration of CHGB proteins within the ER-Golgi network. These results suggest that the P413L missense variation can impede the sorting and maturation of CHGB into secretory granules.

Of particular interest is the finding that ALS patients carrying the P413L *CHGB* variant developed disease nearly 10 years earlier than ALS patients without this variation. This is the first genetic variation documented to influence the age of onset in ALS, both familial and sporadic. Although the exact mechanism by which the P413L *CHGB* variation may act as a risk factor for ALS and a modifier of disease onset remains to be elucidated, it is conceivable that protein misfolding because of amino acid substitution could interfere with the normal signal-mediating sorting of CHGB. There is a short disulfide-bonded loop located near the N terminus of CHGB protein that is essential and sufficient for sorting to the regulatory pathway (19). The involvement of disulfide bond formation led to the suggestion that this sorting signal depends upon proper three-dimensional arrangement of its amino acids (19).

There is evidence that dysfunction of the secretory pathway can contribute to increased vulnerability of motor neurons. Fragmentation of the Golgi apparatus (20) and ER stress are hallmarks of degenerating motor neurons in ALS. There is a recent report suggesting that vulnerable motor neurons in ALS are more prone to ER stress (21). Moreover, the ER-Golgi pathway is a predominant site of uptake and age-dependent aggregation of misfolded mutant SOD1 linked to ALS (22). Disturbances of ER-Golgi homeostasis can constitute a severe form of stress that may interfere with central functions of this network, including the folding, processing, and secretion of newly synthesized proteins. In future, it would be of interest to investigate, with the use of cultured cells and transgenic mouse models, whether expression of *CHGB* variants can enhance the accumulation of misfolded SOD1 species in ER-Golgi and accelerate motor neuron degeneration.

Interestingly, our analysis revealed population differences in the frequency of the SNPs associated with *CHGB* and in the risk factor to develop ALS conferred by certain SNPs. For example, in the population of French ancestry, the frequency of the P413L *CHGB* variant was 5% in controls and 17% in ALS patients, conferring a relative risk of 3.3 times greater to develop disease. In contrast, in the Swedish population, the P413L variant was found in 3.6% of control individuals and 5.2% of ALS patients, conferring a risk of 1.5 times greater to develop disease. Thus, in future it will be of interest to determine the impact of the P413L *CHGB* variant on ALS susceptibility and age of onset in cohorts of other ethnic origins.

Methods

Samples from Patients and Controls. All patients were assessed by expert clinicians and gave written informed consent. Diagnosis of ALS was made according to El Escorial ALS diagnostic criteria (23). Peripheral blood from each patient from France and Canada/Quebec (non-SOD1 FALS = 40; SALS = 58) and healthy controls matched for age and ethnicity ($n = 258$) were collected for the initial screen (see Table 1). Another set of samples from 191 nonrelated SALS cases from France and 190 matched controls were also examined when it was not possible to confirm or exclude association between *CHGB* and ALS. Blood from patients and controls of Swedish origin were also collected and used to validate our initial results (non-SOD1 FALS = 61; SOD1 FALS = 40; SALS = 315; Control = 303) (see Table 1). Overall, the non-SOD1 FALS cohort exhibited a mean age of onset of 56 years, a disease duration of 4.4 years, and a male-to-female ratio of 1:1. The mean age of onset of the SOD1-linked FALS cohort was 49 years, exhibited a disease duration of 11.3 years and a male-to-female ratio of 1.5:1. The SALS cohort

exhibited a mean age of onset of 59 years, a disease duration of 3.4 years, and a male-to-female ratio of about 1.5:1.

Variants Detection and Genotyping. DNA was extracted from whole blood and transformed lymphoblastoid cell lines by using standard procedures. Respectively, 12 and 9 PCR primer pairs were designed from genomic DNA to amplify each exon of the *CHGB* genes, including the flanking splice sites (Table S2). Products were PCR-amplified, checked on agarose gels, and then sequenced by using the forward primer for all of the amplicons. The PCR fragment containing variations were also sequenced on the reverse strands. Each of the variants found were also genotyped on our control populations by allele-specific oligomerization, as previously described (24). Variants that were not found in control individuals or found to be increased in ALS patients were also sequenced in our extra set of SALS samples, as well as in our set of Swedish patients and controls to validate our results. The P413L variation for all extra patients and controls were genotyped by restriction enzyme digestion. The P413L variation abolished an MspI restriction site. PCR fragments amplified from DNA of extra patients and controls were digested with MspI (New England BioLabs) and run on agarose gel to confirm the presence or absence of the P413L variation. PCR primer pair were designed to amplify a 500-bp PCR product in which the P413L variation is located in the middle of the PCR fragment (5′-aacgtcagcatggccagtttag-3′ and 3′-gagggtcgtagtatgggttgaaca-5′).

Statistical Analysis. Deviations from Hardy–Weinberg equilibrium were tested by using the observed allele frequency by the χ^2 contingency test (1 degree of freedom). We assessed differences in distribution of alleles and genotypes between the groups (SALS, FALS, and control) by calculating the χ^2 contingency test using the Fisher's exact test, from which we derived *P*-values with one degree of freedom. *P*-values less than 0.04 were considered statistically significant. Odds ratios were also derived only when significant *P*-values were found. Median age of onset and *P*-values derived from the survival curves among patients were calculated by using the log-rank Mantel–Cox test with Graph Pad Prim5 software. Unpaired *t* test (mean ± standard error) was used to calculate and compare the mean age of onset for each group.

Functional Analysis of Nonsynonymous cSNPs. The PolyPhen program (http://genetics.bwh.harvard.edu/pph) and Pmut (http://mmb2.pcb.ub.es:8080/PMut) were used to predict the functional significance of nonsynonymous cSNPs. The PolyPhen method uses sequence, phylogenetic, and structural information to predict the effect of a particular amino acid change. Sequence alignment is used to generate a quantitative PSIC score and this is combined with any available sequence annotation or structural information to generate a qualitative prediction of a SNP as "benign" (PSIC score <0.5), "possibly damaging" (0.5 <PSIC score interval <2.0) and "probably damaging" (PSIC score >2.0) (25). A PSIC score > 0.5 associated with a benign prediction indicates that the studied substitution is rarely or never observed in the protein family. Pmut exploits a computational approach to the prediction of disease-associated amino acid mutations, using only sequence-based information (amino acid properties, evolutionary information, secondary structure and accessibility predictions, and database annotations). Mutations are predicted to be either pathological (score >0.5) or neutral (score <0.5) (26).

Plasmid Construction and Transfection Studies. Mammalian expression vector for human chromogranin B tagged with EGFP (pEGFP-N3-CHGB) was generated as previously described (8). Two *CHGB* H230R and P413L sequence variations were introduced within the pEGFP-N3-CHGB plasmid by site-directed mutagenesis according to the manufacturer protocol (Agilent technologies, Stratagene division). PCR products obtained from WT pEGFP-N3-CHGB were digested by DpnI and subsequently transformed into *Escherichia coli* DH5alpha competent cells. The PCR primer pairs used for the site directed mutagenesis were: 5′-ttctcaggagaagacacgtagccgagagaagagta-3′ and 5′-tactcttctctcggctacgtgtcttctcctgagaa-3′ for H230R; 5′-ggggccttgagctgggaaagggacg-3′and 5′-cgtccctttcccagctcaaggcccc-3′ for P413L. For cell transfections, human neuroblastoma cell-line SHSY-5Y was cultured in DMEM containing 15% FBS, nonessential amino acids (Invitrogen) and antibiotic (penicillin/streptomycin; Invitrogen) at 37 °C in 5% CO_2 and 100% humidified condition. Cells were transfected by using Lipofectamine plus (Invitrogen) according to the manufacturer's protocol and were counted under epifluorescence microscope. Statistical analysis was done by using one-way ANOVA test and *P* values were then derived.

ACKNOWLEDGMENTS. We thank all families and patients involved in this study. We thank Anne Desjarlais and Pierre Provencher for sample collection and organization, and Christine Bareil, Pascale Hince, Sandra Laurent, Julie Roussel, and Geneviève Soucy for technical support; the French Study Group on motor neuron diseases; and the Association pour la Recherche sur les Maladies du Motoneurone for DNA collection. This work was supported by the ALS Association USA, the ALS Society of Canada, the Canadian Institutes of Health Research, the Muscular Dystrophy Association, l'Association Française contre les Myopathies France, et l'Association pour la Recherche sur la Sclérose Latérale Amyotrophique.

1. Tandan R, Bradley WG (1985) Amyotrophic lateral sclerosis: Part 1. Clinical features, pathology, and ethical issues in management. *Ann Neurol* 18:271–280.
2. Mulder DW, Kurland LT, Offord KP, Beard CM (1986) Familial adult motor neuron disease: amyotrophic lateral sclerosis. *Neurology* 36:511–517.
3. Pramatarova A, et al. (1995) Identification of new mutations in the Cu/Zn superoxide dismutase gene of patients with familial amyotrophic lateral sclerosis. *Am J Hum Genet* 56:592–596.
4. Eisen A, et al. (2008) SOD1 gene mutations in ALS patients from British Columbia, Canada: clinical features, neurophysiology and ethical issues in management. *Amyotroph Lateral Scler* 9:108–119.
5. Bruijn LI, et al. (1998) Aggregation and motor neuron toxicity of an ALS-linked SOD1 mutant independent from wild-type SOD1. *Science* 281:1851–1854.
6. Gurney ME, et al. (1994) Motor neuron degeneration in mice that express a human Cu,Zn superoxide dismutase mutation. *Science* 264:1772–1775.
7. Reaume AG, et al. (1996) Motor neurons in Cu/Zn superoxide dismutase-deficient mice develop normally but exhibit enhanced cell death after axonal injury. *Nat Genet* 13:43–47.
8. Urushitani M, et al. (2006) Chromogranin-mediated secretion of mutant superoxide dismutase proteins linked to amyotrophic lateral sclerosis. *Nat Neurosci* 9:108–118.
9. Ezzi SA, Urushitani M, Julien JP (2007) Wild-type superoxide dismutase acquires binding and toxic properties of ALS-linked mutant forms through oxidation. *J Neurochem* 102:170–178.
10. Schrott-Fischer A, et al. (2009) Chromogranin peptides in amyotrophic lateral sclerosis. *Regul Pept* 152:13–21.
11. Obayashi K, et al. (2008) Salivary chromogranin a: useful and quantitative biochemical marker of affective state in patients with amyotrophic lateral sclerosis. *Intern Med* 47:1875–1879.
12. Giess R, et al. (2002) Early onset of severe familial amyotrophic lateral sclerosis with a SOD-1 mutation: potential impact of CNTF as a candidate modifier gene. *Am J Hum Genet* 70:1277–1286.
13. Lambrechts D, et al. (2003) VEGF is a modifier of amyotrophic lateral sclerosis in mice and humans and protects motoneurons against ischemic death. *Nat Genet* 34:383–394.
14. van Es M, et al. (2009) Genome-wide association study identifies 19p13.3 (UNC13A) and 9p21.2 as susceptibility loci for sporadic amyotrophic lateral sclerosis. *Nat Genet* 41:1083–1087.
15. Scharf JM, et al. (1998) Identification of a candidate modifying gene for spinal muscular atrophy by comparative genomics. *Nat Genet* 20:83–86.
16. Strittmatter WJ, et al. (1993) Apolipoprotein E: high-avidity binding to beta-amyloid and increased frequency of type 4 allele in late-onset familial Alzheimer disease. *Proc Natl Acad Sci USA* 90:1977–1981.
17. van Duijn CM, et al. (1994) Apolipoprotein E4 allele in a population-based study of early-onset Alzheimer's disease. *Nat Genet* 7:74–78.
18. Corder EH, et al. (1993) Gene dose of apolipoprotein E type 4 allele and the risk of Alzheimer's disease in late onset families. *Science* 261:921–923.
19. Kromer A, Glombik MM, Huttner WB, Gerdes HH (1998) Essential role of the disulfide-bonded loop of chromogranin B for sorting to secretory granules is revealed by expression of a deletion mutant in the absence of endogenous granin synthesis. *J Cell Biol* 140:1331–1346.
20. Mourelatos Z, et al. (1990) Fragmentation of the Golgi apparatus of motor neurons in amyotrophic lateral sclerosis revealed by organelle-specific antibodies. *Proc Natl Acad Sci USA* 87:4393–4395.
21. Saxena S, Cabuy E, Caroni P (2009) A role for motoneuron subtype-selective ER stress in disease manifestations of FALS mice. *Nat Neurosci* 12:627–636.
22. Urushitani M, Ezzi SA, Matsuo A, Tooyama I, Julien JP (2008) The endoplasmic reticulum-Golgi pathway is a target for translocation and aggregation of mutant superoxide dismutase linked to ALS. *FASEB J* 22:2476–2487.
23. Brooks BR, Miller RG, Swash M, Munsat TL (2000) El Escorial revisited: revised criteria for the diagnosis of amyotrophic lateral sclerosis. *Amyotroph Lateral Scler Other Motor Neuron Disord* 1:293–299.
24. Labuda D, et al. (1999) Rapid detection of CYP1A1, CYP2D6, and NAT variants by multiplex polymerase chain reaction and allele-specific oligonucleotide assay. *Anal Biochem* 275:84–92.
25. Sunyaev S, et al. (2001) Prediction of deleterious human alleles. *Hum Mol Genet* 10:591–597.
26. Ferrer-Costa C, Orozco M, de la Cruz X (2004) Sequence-based prediction of pathological mutations. *Proteins* 57:811–819.

Neuroscience 164 (2009) 1565–1578

AXONAL LIGATION INDUCES TRANSIENT REDISTRIBUTION OF TDP-43 IN BRAINSTEM MOTOR NEURONS

T. SATO,[a,c] S. TAKEUCHI,[a] A. SAITO,[a,c] W. DING,[b] H. BAMBA,[c] H. MATSUURA,[b] Y. HISA,[c] I. TOOYAMA[a] AND M. URUSHITANI[a]*

[a]*Molecular Neuroscience Research Center, Shiga University of Medical Science, Seta-Tsukinowa-cho, Otsu, Shiga 520-2192, Japan*

[b]*Department of Physiology, Shiga University of Medical Science, Seta-Tsukinowa-cho, Otsu, Shiga 520-2192, Japan*

[c]*Department of Otolaryngology-Head and Neck Surgery, Kyoto Prefectural University of Medicine, Kawaramachi-Hirokoji, Kyoto 602-8566, Japan*

Abstract–Nuclear exclusion of TAR DNA binding protein 43 (TDP-43) and formation of cytosolic aggregates are a pathological characteristic of amyotrophic lateral sclerosis (ALS). However, the molecular basis of the aberrant distribution of TDP-43 remains elusive. Here, we show evidence that axonal ligation induced transient nuclear exclusion and peripheral accumulation of TDP-43, without apparent cytosolic aggregates in hypoglossal neurons in mice. Immunohistochemistry showed marked loss of nuclear TDP-43 7–14 days after ligation, which was accompanied by reduction of choline acetyltransferase (ChAT). TDP-43 staining was restored in the nucleus on day 28 exclusively in the neurons with normalized ChAT expression. We also showed that importin β, which was shown to mediate nuclear transport of TDP-43 was downregulated transiently by nerve ligation. The analysis of the peripheral nerves proximal to the ligation revealed that TDP-43 markedly accumulated with a concomitant decrease in active autophagosome. Moreover, we showed that TDP-43 was present in the microsome fraction containing endoplasmic reticulum (ER) or autophagosomes in the brainstem section, indicating that TDP-43 is axonally transported with vesicles. These results indicate that axonal damage is associated with redistribution of TDP-43 through the combination of defective axonal autophagy periphery and the impaired nuclear transport system in the soma. Moreover, it was also shown that transient redistribution of TDP-43 does not prevent motor neurons from axonal regeneration. Therefore, our data suggest that the subcellular distribution of TDP-43 correlates to the innervation status of motor neurons, which may be governed by unidentified cause of ALS.

Key words: amyotrophic lateral sclerosis (ALS), TAR DNA binding protein 43 (TDP-43), hypoglossal nerve, importin, choline acetyltransferase (ChAT), axonal flow.

TAR DNA binding protein 43 (TDP-43) is a nuclear protein with unknown function, which to date, is recognized as a pathological and biochemical marker for frontotemporal lobar degeneration with ubiquitin inclusion (FTLD-U) and amyotrophic lateral sclerosis (ALS) (Arai et al., 2006; Neumann et al., 2006; Kwong et al., 2007). Although the nuclear exclusion and the cytosolic aggregates are typical findings in most ALS patients (Arai et al., 2006; Neumann et al., 2006; Dickson et al., 2007), the role of TDP-43 mislocalization in the ALS pathogenesis is unclear. Strikingly, the genetic mutations in TDP-43 were discovered in both familial and sporadic ALS patients (Gitcho et al., 2008; Kabashi et al., 2008; Sreedharan et al., 2008; Yokoseki et al., 2008). However, the motor neuron death caused by mutant TDP-43 is not necessarily related to its mislocalization (Sreedharan et al., 2008).

Currently, it is unclear how and why mislocalization of TDP-43 is induced. It should be noted that the mislocalization of TDP-43 is not a general outcome of cytotoxic events according to a report by Lee et al, in which TDP-43 is normally stained in autopsy specimens from patients with anoxia, ischemia, or whose hippocampus was resected for epilepsy (Lee et al., 2008). Intriguingly, Zhang et al reported that TDP-43 is a substrate for caspases, in which caspase-cleaved TDP-43 is excluded from the nucleus (Zhang et al., 2007). TDP-43 carries a bipartite nuclear localization signal (NLS; KRKXXXXXXXXXXXXKR) at 82–98 amino acids, and a defect in this signal prevents the nuclear transport of TDP-43 (Winton et al., 2008). The authors also demonstrated that cytosolic TDP-43 induces sequestration of normal endogenous TDP-43 to the cytoplasm. Furthermore, recent paper documented that TDP-43 with defective NLS is readily phosphorylated and aggregated in the cytosol (Nonaka et al., 2009).

The bipartite NLS is a universal sequence, which is recognized by importin α/β (also known as karyopherin) (Otis et al., 2006). In particular, accumulating evidence has clarified a crucial role of importin β in the nuclear transport of most proteins (Pouton et al., 2007). In the nucleus, importing β interacts with Ran-GTP, which is important for recycling importin β and Ran-GDP in the cytosol. To date, there has been no report describing the relationship between TDP-43 and importins. Interestingly, importin β is shown to function in neuronal regeneration upon axonal injury, in which local expression of importin β at the lesion site promotes neuronal survival via facilitating the nuclear transport of cytoprotective molecules such as pErk (Hanz et al., 2003; Perlson et al., 2005). Since axonal flow damage is a major pathological feature in ALS (Julien, 2001), the effect of axonal damage on TDP-43 abnormality deserves exploration. Recently, Moisse et al have reported that sciatic axotomy induced cytosolic redistribution of TDP-43 in the spinal motor neurons

*Corresponding author. Tel: +81-77-548-2402; fax: +81-77-548-2402.
E-mail address: uru@belle.shiga-med.ac.jp (M. Urushitani).

Abbreviations: ALS, amyotrophic lateral sclerosis; ChAT, choline acetyltransferase; DAB, diaminobenzidine; LCM, laser capture microdissection; LC3, microtubule-associated protein1 light chain 3; TDP-43, TAR DNA binding protein 43.

0306-4522/09 $ - see front matter
doi:10.1016/j.neuroscience.2009.09.050

(Moisse et al., 2009). This phenomenon was preceded by upregulation of TDP-43 in the spinal cord hemi-section. Moreover, nuclear-excluded TDP-43 colocalized with RNA transport markers and stress granules, indicating TDP-43 plays a role in sequestering and regulating mRNA level in response to axonal injury. However, molecular basis of redistribution of TDP-43, especially in the pure motor neurons suffering axonal damage is unknown.

Here, we investigated the effect of axonal ligation of hypoglossal nerves on the subcellular localization of TDP-43, focusing on ChAT and nucleocytoplasmic transport system. We found that aberrant TDP-43 is a downstream phenomenon to more pathogenic events related to axonal damage.

EXPERIMENTAL PROCEDURES

Antibodies

Detailed information on the antibodies regarding the company, dilution, application, and references is available in the supplementary table. We also generated rabbit polyclonal antibody against the carboxyl terminus of human/mice TDP-43 (TDP-Ct) using a conventional immunization protocol. In brief, KLH-conjugated peptides with the sequence of CGSGFNGGFGSSMDSKSSGWGM were used to immunize two rabbits four times. One of the two antisera obtained was further affinity-purified using an antigen peptide-cross-linked column (sulfolink, Pierce, Rockford, IL, USA).

Animals, surgery, and tissue sampling

All experimental protocols were performed respecting the dignity of animal lives and were approved by the animal experimental committee of Shiga University of Medical Science (# 2007-8-2). Adult C57Bl/6 mice were subjected to deep anesthesia with 1.5%~2.0% of isoflurane. The hypoglossal nerve was tightly ligated 5 mm proximal to bifurcation before insertion to the tongue with 6-0 silk suture. Mice were placed into a warm cage until moving, and then housed back in conventional conditions until analysis. Unilateral ligation or axotomy of the hypoglossal nerve did not cause any serious defect in the mice such as loss of activity, food intake or body weight. Mice were sacrificed for analysis at 1, 5, 7, 14 and 28 day after surgery as indicated in the Results section. Mice were perfused with 0.1 M phosphate buffer (PB) alone for laser capture microdissection (LCM) and hypoglossal nerve resection, or with PB with 4% paraformaldehyde (PFA) for immunohistochemistry. Sections were prepared at 10 or 20 μm-thickness for LCM or immunohistochemistry, respectively, using the cryostat (Leica, Nussloch, Germany).

Histochemistry or immunocytochemistry

After quenching endogenous peroxidase by incubation in 1% H_2O_2 for 10 min, the brainstem slices were reacted with primary antibody overnight at 4 °C, then with biotin-conjugated secondary antibody (Vector, Burlingame, CA, USA) for 1 h at room temperature, and finally detected by diaminobenzidine (DAB) using an avidin-biotin complex system (Vector). For double staining, slices were incubated with a mixture of primary antibodies, and subsequently with a mixture of corresponding secondary antibodies labeled with Alexa 488 or 594 (Invitrogen, Carlsbad, CA, USA). For counter-staining, bis-benzimide H33342 (Hoechst 33342, Invitrogen), 4,6-Diamidino-2-phenylindole dihydrochloride (DAPI, Nacalai Tesque, Kyoto, Japan) and Cresyl Violet (Sigma, St. Louis, MO, USA) was used for live cell imaging, immunofluorescence staining and DAB staining, respectively. Fluorescent images were obtained using a confocal laser microscope equipped with the software EZ-C1 (Nikon, Tokyo, Japan).

Cell counting

The population of hypoglossal nucleus showing aberrant TDP-43 staining was obtained by counting under microscope observation or micrographs. The hypoglossal nucleus with normal TDP-43 staining and Nissl-positive hypoglossal nucleus was counted on the control or the ligation side from three slices per mouse from three to four mice. The population of hypoglossal nucleus with normal TDP-43 staining under axonal ligation was expressed as percent to the control side. Difference was estimated by one-way ANOVA of Bonferroni test. In case of the confocal microscope, the photographs were obtained first and hypoglossal nucleus or choline acetyltransferase (ChAT)-positive, labeled in green or red, respectively, were counted from three slices per mouse from three mice. Data were expressed as mean±standard error of mean (SEM). The difference was evaluated using Student's *t*-test.

In situ hybridization

Brainstem slices at 20 μm-thickness at the medulla level were mounted on aminopropyl triethoxysilane (APS)-coated glass coverslips and digested with 10 μg/ml proteinase K for 25 min at 37 °C. Sections were washed in diethylpyrocarbonate-treated distilled water, subsequently in 0.1 M triethanolamine (TEA) pH 8.0, and acetylated in 0.1 M TEA containing 0.25% acetic acid. After two washes in 2X SSC, sections were incubated in prewarmed prehybridization buffer (50% formamide in 2X SSC) for 30 min, and subsequently in hybridization solution (*see below*) at 60 °C overnight. The next day, sections were washed three times in prehybridization buffer, and reacted with 20 mg/ml RNase for 30 min at 37 °C. After washing three times in 0.1X SSC at 42 °C and blocking in 1% skimmed milk, the samples were processed to overnight incubation with an alkaline phosphatase-conjugated anti-DIG antibody at 4 °C. On day 3, mRNA was colorized by reaction with 0.5 mg/ml nitro blue tetrazolium (NBT) and 0.18 mg/ml 5-Bromo-4-Chloro-3'-Indolylphosphatase p-Toluidine salt (BCIP).

For cRNA probe synthesis, a 580 bp fragment was subcloned into a pcDNA3 vector (Invitrogen) between the T7 and SP6 promoter sequences. The primer pairs for cloning the probe are; 5'-TCTGACCTCATAGTGTTGGGT-3' and 5'-TCCCTCCACCCATATTACCA-3' for mouse TDP-43. Plasmids were linearized by digestion with BamHI for antisense probe and XhoI for sense probe. Digoxygenin (DIG)-labeled cRNA probes were generated using a commercially available kit (Roche, Basel, Switzerland) according to the manufacturer's protocol, in which SP6 RNA polymerase is used for the antisense probe and T7 RNA polymerase for the sense probe.

Laser capture microdissection and real-time RT-PCR

Messenger RNA for TDP-43 in the hypoglossal nucleus of the mice on day 0 and 7 after the ligation was assessed by quantitative real-time PCR in the isolated hypoglossal nucleus using a LCM system. Pre-chilled slices at 10 μm-thickness were placed onto non-coated glass slides, fixed in 75% ethanol, and rinsed in RNase-free distilled water. After dehydration by serial incubation in 75–95–100% ethanol–xylene, sections were stained with Cresyl Violet to visualize the hypoglossal nucleus. The LCM system was performed using a PixCell II microscope (Arcturus, Engineering, Mountain view, CA, USA) with CapSure LCM microcaps (Arcturus). Using about 1500 cells collected from serial sections on the operated or control side, total RNA was purified using a commercially available kit (Picopure RNA isolation kit, Arcturus), and then cDNA was generated by reverse transcriptase reaction using a mixture of oligodT and random primers (PrimeScript RT reagent Kit, Takara, Kyoto, Japan). Real time PCR was conducted on a LightCycler system (Roche, Basel, Switzerland) using the intercalator method with SYBR green I (Takara, Kyoto, Japan) according to the manufacturer's protocol.

Briefly, relative quantification of TDP-43, importin β or actin was performed using the standard curve generated from simultaneous PCR run with the plasmid carrying each cDNA. To correct for run-to-run and sample-to-sample variation, mRNA levels of TDP-43 or importin β were normalized to the level of actin mRNA in the same RCR run, and the mRNA level for TDP-43 or importin β was expressed as fold increase versus actin. Each value was expressed as the mean ratio of TDP-43 or importin β to actin in three mice. TDP-43/actin or importin β/actin ratio of the ligation side from three mice was obtained by the comparison with the control side, and was expresses as fold-increase of the control. The primer pairs were as followings; 5′-CCTTCGTCACCTTTGCAGAT-3′ and 5′-TCCCTCCACCCATATTACCA-3′ for mouse TDP-43, 5′-GCTTATACGGGAATCGTCCA-3′ and 5′-CCTATCAGACCAGCAGCACA-3′ for importin β and 5′-TGGTGGGCATGGGTCAGAAGGATTC-3′ and 5′-CATGGCTGGGGTGTTGAAGGTCTCA-3′ for actin.

Plasmid construction

cDNA of human TDP-43 was cloned from the messenger RNA of human embryonic kidney (HEK) 293 cells using a commercially available RNA purification kit (RNeasy, Qiagen, Venlo, Netherland) and the reverse transcriptase PCR technique (Invitrogen, Carlsbad, CA, USA). Next, a TDP-43-FLAG fragment was generated by PCR using primer pairs, 5′-GGCGGATCCAAGATGTCTGAATATATTCGG-3′ and 5′-GGCCTCGAGTCACTTGTCGTCATCGTCTTTGTAGTCCATTCCCCAGCCAGAAGA-3′. The PCR product was cloned once using a TA cloning kit (Invitrogen), and then a doubly digested fragment was ligated into a pcDNA3 vector (Invitrogen) at the BamHI and XhoI sites (named pcDNA3-TDP-43-FLAG). To generate a plasmid expressing EGFP-fused TDP-43, PCR products derived from the primer pairs, 5′-GGCCTCGAGAAGATGTCTGAATATATTCGG-3′ and 5′-GGCGGATCCCATTCCCCAGCCAGAAGAC-3′ were introduced into the pEGFP-N3 vector (Clontech, Palo Alto, CA, USA) at the XhoI/BamHI sites (named pEGFP-TDP-43).

Nucleotide sequence and protein expression were verified by DNA sequencing and Western blotting, respectively.

Cell culture and transfection of plasmid or siRNA

Human neuroblastoma cell-line SHSY-5Y cells were a generous gift from Julie Goemaere, Université Catholique de Louvain, Belgium, and were cultured in DMEM/F12-Ham medium (Invitrogen) containing 15% fetal bovine serum, 1% non-essential amino acid and penicillin/streptomycin under 5% CO_2 in 100% humidified conditions. To investigate the effect of the nucleocytoplasmic transport system on TDP-43 localization, importin β was knocked down through small interfering RNA (siRNA) using Lipofectamine iMax with subsequent transfection of TDP-43-EGFP using FuGene HD according to the manufacturer's protocol. Briefly, 45 pmol of annealed siRNA together with 1 μl Lipofectamine iMax (Invitrogen) was introduced into SHSY-5Y cells which had been plated onto a 24 multi-well culture dish or Lab-Tek culture plate. The next day, 0.5 μg of pEGFP-N3-TDP-43 plasmid with 1.5 μl of FuGene HD (Roche, Basel, Switzerland) was further transfected. Cells were analyzed at 48 h after plasmid transfection for live cell imaging using confocal laser microscope, or Western blotting. The sequence of the siRNA is 5′-UAAACUCUCCUCCAAUAGCAAGGGC-3′(siRNA1), 5′-AUCCCUGGACGAUUCCAGUAUAGGC-3′ (siRNA2), 5′ UUGAUUUGUAGACCAGCUGCAACUC 3′ (siRNA3) and complementary oligonucleotides for each. Random siRNA were purchased from Invitrogen (universal negative control) as negative controls. For the biochemical analysis of the subcellular localization of TDP-43 under RNA knockdown, siRNA and pcDNA3-TDP-43-FLAG were transfected using the same protocol as above.

Sampling of hypoglossal nerves and brainstem hemi-sections for Western blotting

Hypoglossal nerves of 1.5-cm long with the ligation at the midpoint were resected to obtain both the treated and the contralateral side 7 days after ligation. Nerves that were 5 mm distal or proximal to the ligation point (Fig. 6A), were pooled from 3 mice and homogenized in urea buffer (7 M urea, 2 M Thiourea, 4% CHAPS, 0.5% SDS in 30 mM Tris–HCl, pH 8.5). The nerve stump around the ligation site was omitted due to possible contamination with reactive glial cells or other connective tissues. As controls, the opposite hypoglossal nerves corresponding to the resected parts were collected as well. After removing debris by centrifugation at 17,400 g for 20 min, supernatants were denatured in 2% SDS-sampling buffer at 75 °C for 15 min, and analyzed by Western blotting using antibodies against TDP-43 (Proteintech), importin β, glyceraldehyde-3-phosphate dehydrogenase (GAPDH) and actin. For the analysis of brain tissues, the brainstem sections at the level of the lower medulla were separated into the control (left) or the ligation side (right). After homogenization in RIPA buffer (20 mM HEPES pH 7.4, 150 mM NaCl, 2 mM EDTA, 1% nonidet-P40, 1% sodium deoxycholate, 0.1% SDS, and protease inhibitor cocktail) and the sonication, the homogenates were centrifuged at 17,400 g ×20 min at 4 °C, and the supernatant was analyzed after the protein quantification using Bradford method.

To investigate whether the TDP-43 is present in the luminal structure, microsome fraction from the hemi-section of brainstem slices with or without hypoglossal ligation was analyzed. On day 7 after the nerve ligation, mice were perfused with PBS, and the hemi-section of the brainstem at the medulla level was resected and two hemi-sections were mixed. The tissue lysates were obtained using Dounce homogenizer in the homogenization buffer (10 mM HEPES, pH 7.4, 10 mM PBS, 0.25 M sucrose, 1 mM $MgCl_2$, and protease inhibitor cocktail). Then, the lysates were subcellularly fractionated as described previously (Urushitani et al., 2006). In brief, the samples were sequentially centrifuged at 1000×*g* and 10,000×*g* for 5 min at 4 °C to exclude nucleus and mitochondria fraction, respectively. The final supernatant (S1) were equally divided into five tubes, and ultracentrifuged at 100,000×*g* for 1 h at 4 °C. The resulting pellets (microsomes) were resuspended in 10 mM Tris–HCl (pH 7.4) containing 0, 0.1, 0.5, 1.0 M of NaCl, and were ultracentrifuged again. The supernatant was replaced to 1×SDS sampling buffer, and denatured at 95 °C for 5 min. The samples were analyzed by Western blotting using antibodies against TDP-43 (TDP-Ct), LC3, and calnexin.

To further test the possibility that TDP-43 is transported via trans-Golgi network (TGN), the TGN was immunoisolated from the brainstem hemi-section using previously reported protocol with minor modifications (Urushitani et al., 2006). The S1 supernatant was incubated with protein G-coated magnetic beads (Dynabeads, Invitrogen), which was previously cross-linked with anti-TGN38 antibody in the homogenization buffer containing 1% BSA overnight at 4 °C. The absorbed proteins were eluted in the 4% SDS sampling buffer without a reducing agent at 95 °C for 5 min. The eluates were reacted with 100 mM dithiothreitol (DTT) for 5 min at 95 °C again. The samples were analyzed by Western blotting using anti-TDP-43 (TDP-Ct) or anti-TGN38 antibody.

Western blotting

Tissue lysates were denatured in SDS sampling buffer at 95 °C for 5 min. Samples were separated in 10–20% gradient polyacrylamide gels (Wako, Osaka, Japan), and were transferred onto PVDF membrane (Millipore, Billerica, MA, USA). Target proteins labeled by primary and peroxidase-conjugated secondary antibodies (Jackson immunoresearch, West Grove, PA, USA) were visualized using an enhanced chemiluminescence detection kit (West Pico, Pierce, Rockford, IL, USA), using a lumino image analyzer (LAS-4000, Fuji, Tokyo). For densitometric analysis, ImageJ software was used to quantify Western bands.